
ΔEnergy: Optimizing Energy Change During Vision-Language Alignment Improves both OOD Detection and OOD Generalization

Lin Zhu¹, Yifeng Yang¹, Xinbing Wang¹, Qinying Gu², Nanyang Ye¹ *

¹ Shanghai Jiao Tong University, ² Shanghai Artificial Intelligence Laboratory
 {zhulin_sjtu, xwang8, ynylincoln}@sjtu.edu.cn,
 maxwellquadyang@gmail.com
 guqinying@pjlab.org.cn

Abstract

Recent approaches for vision-language models (VLMs) have shown remarkable success in achieving fast downstream adaptation. When applied to real-world downstream tasks, VLMs inevitably encounter both the in-distribution (ID) data and out-of-distribution (OOD) data. The OOD datasets often include both covariate shifts (e.g., known classes with changes in image styles) and semantic shifts (e.g., test-time unseen classes). This highlights the importance of improving VLMs' generalization ability to covariate-shifted OOD data, while effectively detecting open-set semantic-shifted OOD classes. In this paper, inspired by the substantial energy change observed in closed-set data when re-aligning vision-language modalities—specifically by directly reducing the maximum cosine similarity to a low value—we introduce a novel OOD score, named ΔEnergy. ΔEnergy significantly outperforms the vanilla energy-based OOD score and provides a more reliable approach for OOD detection. Furthermore, ΔEnergy can simultaneously improve OOD generalization under covariate shifts, which is achieved by lower-bound maximization for ΔEnergy (termed EBM). EBM is theoretically proven to not only enhance OOD detection but also yields a domain-consistent Hessian, which serves as a strong indicator for OOD generalization. Based on this finding, we developed a unified fine-tuning framework that allows for improving VLMs' robustness in both OOD generalization and OOD detection. Extensive experiments on challenging OOD detection and generalization benchmarks demonstrate the superiority of our method, outperforming recent approaches by **10%–25%** in AUROC.

1 Introduction

Recent advances in pre-trained vision-language models (VLMs), such as CLIP (Radford et al., 2021), VLMo (Bao et al., 2022), MiniGPT-4 (Zhu et al., 2023a), etc., have shown promising results in visual-semantic learning. However, downstream use cases often involve further fine-tuning of VLMs. When applied to real-world downstream tasks, VLMs inevitably face challenges related to out-of-distribution (OOD) data, stemming from differences in data distributions between the training and test sets (Meinshausen and Bühlmann, 2015; Koh et al., 2020). As illustrated in Figure 1, these OOD datasets often involve *closed-set OOD* data that exhibit *covariate shifts* (i.e., changes in environments, while class labels remain the same as the in-distribution data), as well as *open-set OOD* data with *semantic shifts* (i.e., test-time new categories that were unseen during fine-tuning). It is crucial to distinguish these unknown categories from known ones, rather than blindly predicting them as known classes (Wang et al., 2023b,a). Therefore, it is essential to *develop robust models that enhance VLMs'*

*Nanyang Ye is the corresponding author.

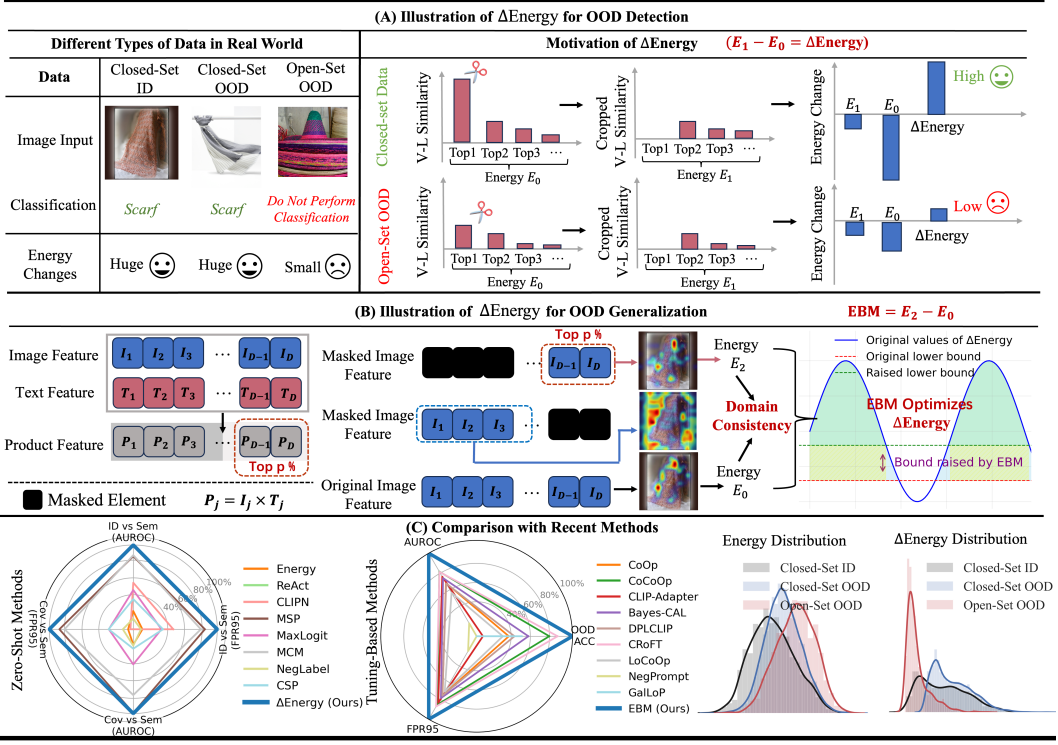


Figure 1: (A) Illustration of Δ Energy for OOD detection. Significant differences in Δ Energy are observed between closed-set data and open-set OOD data when the maximum cosine similarity is cropped to zero. (B) Illustration of the Δ Energy for OOD generalization. We introduce the EBM method to achieve domain-consistent Hessians, which simultaneously triggers bound optimization for Δ Energy. More details are in Section 3.2. (C) Comparison between our Δ Energy and EBM with state-of-the-art methods. In the radar plots, all values are normalized to the range [0, 1]. It is observed that recent methods aimed at improving VLMs' OOD detection may not scale well to handling different types of distribution shifts in challenging ImageNet-1k OOD datasets.

generalization ability to closed-set OOD data, while also effectively detecting open-set OOD classes during fine-tuning.

However, most previous studies (Wortsman et al., 2022; Chen et al., 2024; Jiang et al., 2023; Goyal et al., 2023; Wang et al., 2023a; Ming et al., 2022a; Bai et al., 2024; Li et al., 2024a) have primarily focused on improving VLMs' robustness to training classes or developing OOD detection method for unseen classes independently. Consequently, existing approaches are often highly specialized for a single task and are not capable of simultaneously addressing both aspects. Recent works (Yang et al., 2023; Zhang et al., 2023a) have taken into account both shift types and introduced full-spectrum OOD (FS-OOD) detection, which considers both detecting semantic shifts and being tolerant to covariate shifts. While the FS-OOD benchmark evaluates OOD detection performance across various distribution types, it may not focus on improving VLM's classification accuracy on covariate-shifted data. Several studies (Lafon et al., 2024; Zhu et al., 2024, 2025a) also have attempted to tackle this issue using multiple diverse prompts or through energy optimization techniques. However, these approaches (Lafon et al., 2024; Zhu et al., 2024) often require significantly more computational resources to train additional local prompts or have been evaluated on a narrow set of post-hoc functions for OOD detection. Thus, when fine-tuning VLMs for downstream tasks, the challenge of improving the VLMs' generalization ability to closed-set OOD data while simultaneously detecting open-set OOD classes that were unseen during fine-tuning remains largely underexplored.

In this paper, we develop novel zero-shot and few-shot fine-tuning paradigms to go beyond the limitations of previous studies. We begin by proposing a new post-hoc OOD detection method, inspired by the following heuristic observation: Given the text prompts corresponding to ID data and input images, we compute the cosine similarities between the image features and text features. As shown in Figure 1 (A), when we crop the maximum cosine similarity to a low value (such as by

resetting to zero), the resulting change in energy score (Liu et al., 2020) is substantially different between closed-set data and open-set semantic-shifted classes.

Takeaways for Δ Energy when aligning vision language modalities

When re-aligning vision-language modalities by setting the maximum cosine similarity to zero, we define the resulting change in energy score as Δ Energy. As demonstrated in Theorem 3.2, the Δ Energy for ID data is consistently larger than that for OOD data, indicating that it provides a discriminative and effective method for OOD detection. Meanwhile, compared to the MCM method and raw energy scores, Δ Energy amplifies the difference between ID and OOD data—a property supported by both theoretical analysis and empirical evidence. Extensive experiments further demonstrate that our method outperforms state-of-the-art zero-shot OOD detection approaches on hard OOD detection benchmarks.

Building on this insight, we propose leveraging the energy change to distinguish closed-set classes from open-set OOD classes. We introduce a zero-shot OOD detection method, termed Δ Energy, which quantifies the energy change resulting from modifying vision-language alignment (i.e., the cosine similarities). As demonstrated in Section 4, Δ Energy significantly outperforms recent methods in detecting hard OOD classes, providing a more reliable approach for OOD detection.

Moreover, Δ Energy can be further optimized to enhance OOD detection while simultaneously improving OOD generalization. This is achieved through Δ Energy-based bound maximization (termed EBM) during few-shot adaptation of VLMs. As depicted in Figure 1 (B), we modify the vision-language alignment by retaining the $p\%$ of the image feature elements (with p as a hyperparameter) and masking the remaining elements. The resulting masked features are then used to compute a new energy change between the original and masked models, which we refer to as EBM. As demonstrated in Theorem 3.4, minimizing EBM is theoretically shown to maximize the lower bound of Δ Energy. Moreover, the EBM method not only theoretically enhances the discrimination between closed-set known classes and open-set OOD classes based on the newly introduced OOD score (See Theorem 3.4), but also leads to stronger OOD generalization under covariate shifts (See Theorem 3.5). This allows us to fine-tune VLMs in a unified framework, enhancing both OOD generalization for closed-set OOD data and OOD detection for open-set OOD data.

2 Preliminary

In this section, we first provide the data setting in Notation 2.1 and formally define the target tasks. Based on the widely-used vision-language model CLIP (Radford et al., 2021), we then present the motivation for modifying the vision-language alignment through a masking operation.

Notation 2.1. Given the in-distribution (ID) samples from the downstream task, $\{\mathbf{x}_i, \mathbf{y}_i\}_{i=1}^N$, we define the classes of these samples as closed-set classes, while the other classes are considered as open-set OOD classes. The text prompts for the closed-set classes are defined as $\mathcal{T}_{\text{in}} = \{t_1, t_2, \dots, t_K\}$, where K represents the number of closed-set classes. Each text prompt t_i can be formulated as “a photo of a {CLASS NAME}”. Based on a pre-trained VLM, we can obtain the zero-shot image features and text features, denoted as $\{\mathbf{z}_I(\mathbf{x}_i)\}_{i=1}^N$ and $\{\mathbf{z}_T(t_i)\}_{i=1}^K$, respectively. Both $\mathbf{z}_I(\mathbf{x}_i)$ and $\mathbf{z}_T(t_i)$ are D -dimensional features.

Task definition Given a set of *closed-set ID* samples $\{\mathbf{x}_i, \mathbf{y}_i\}_{i=1}^N$, drawn from a source domain \mathcal{S} , the model is tasked with learning a robust predictor $f : \mathcal{X} \rightarrow \mathcal{Y}$, which maps inputs $\mathbf{x} \in \mathcal{X} = \mathbb{R}^{D_0}$ to outputs $\mathbf{y} \in \mathcal{Y} = \mathbb{R}^K$, where D_0 is the dimension of \mathbf{x} and K is the class number. Here, N is the total number of the few-shot ID samples. To effectively address both closed-set OOD data (covariate shifts) and open-set OOD data (semantic shifts), we aim to enhance the robustness of predictor f from two perspectives: 1) *OOD generalization*, which requires the model to generalize on closed-set classes from new domains \mathcal{T} that exhibit covariate shifts; and 2) *OOD detection*, which enables the model to detect open-set OOD classes during test time.

Effect of vision-language re-alignment through masking We illustrate how vision-language re-alignment is achieved through a specific masking strategy during fine-tuning. Given an image input \mathbf{x}_i and the text prompt t that yields the maximum cosine similarity, we denote the corresponding zero-shot image feature and text feature as $\mathbf{z}_I(\mathbf{x}_i)$ and $\mathbf{z}_T(t)$, respectively. We then compute their

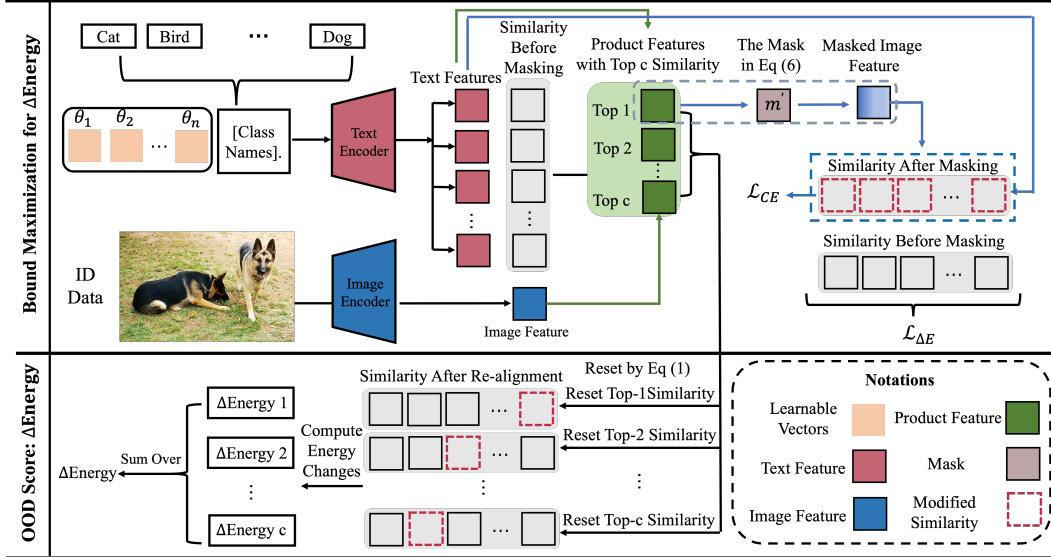


Figure 2: Overview of the proposed method. Based on the prompt-tuning approach, we freeze both the image encoder and the text encoder, making only the context vectors ($\theta = [\theta_1, \dots, \theta_n]$) learnable under the proposed objective function, as shown in Equation 8. During fine-tuning, we apply a masking operation to each ID image feature based on the top-1 similarity, as defined in Equation 6. We then compute the resulting energy change after modifying the vision-language alignment via masking, which allows us to perform bound optimization on ΔEnergy . In the inference phase, following Equation 1, we reset the top- c cosine similarities and then compute ΔEnergy for OOD detection. Simultaneously, we use the fine-tuned text feature and unmasked image feature for classification at test time. The complete algorithm can be seen in Appendix G.

element-wise product, represented as $\mathbf{z}_P(\mathbf{x}_i) := \mathbf{z}_I(\mathbf{x}_i) \odot \mathbf{z}_T(t)$. Let I_j , T_j , and P_j denote the j -th element of $\mathbf{z}_I(\mathbf{x}_i)$, $\mathbf{z}_T(t)$, and $\mathbf{z}_P(\mathbf{x}_i)$, respectively, such that $I_j \cdot T_j = P_j$. Based on the product vector $\mathbf{z}_P(\mathbf{x}_i)$, we mask (zero-out) elements in $\mathbf{z}_I(\mathbf{x}_i)$ where $P_j > 0$. *This masking operation thus effectively reduces the maximum cosine similarity to a low value, achieving modified vision-language alignment.* Moreover, from the attention visualization in Figure 1 (B), the pre-trained VLM initially focuses on the foreground object. However, after masking the elements of the image feature where $P_j > 0$, the model’s attention shifts and becomes more reliant on background information. In contrast, masking the elements where $P_j < 0$ preserves the model’s original attention, which motivates us to leverage this consistency between the original and masked domains to improve OOD generalization. Additional visualizations are provided in Figure 3 in Appendix G.

3 Methodology

Building upon the heuristic observations as shown in Figure 1, we propose a novel OOD score, named ΔEnergy , that measures the energy change when re-aligning vision-language modalities. We theoretically demonstrate that ΔEnergy outperforms the widely-used MCM (Ming et al., 2022a) (see Theorems 3.2-3.3). Moreover, we introduce a ΔEnergy -based bound maximization, which is proven to not only enhance OOD detection (see Theorem 3.4) but also lead to stronger OOD generalization (see Theorem 3.5). Before delving into the details, we provide the notations in this section as follows:

Notation 3.1. We define the cosine similarity ² between the image feature $\mathbf{z}_I(\mathbf{x}_i)$ and text feature $\mathbf{z}_T(t_j)$ as $s_j(\mathbf{x}_i) = \mathbf{z}_I(\mathbf{x}_i) \cdot \mathbf{z}_T(t_j)$. Let $\hat{y}_1 := \text{argmax}_{i \in [K]} s_i(\mathbf{x}_i)$ denote the index of the maximum cosine similarity and $\hat{y}_j := \text{argmax}_{i \in [K] \setminus \{\hat{y}_1, \dots, \hat{y}_{j-1}\}} s_i(\mathbf{x}_i)$ denote the index of the j -th largest cosine similarity. And we denote the corresponding text features that have the j -th largest similarity with $\mathbf{z}_I(\mathbf{x}_i)$, as $\mathbf{h}_j(\mathbf{x}_i) := \mathbf{z}_T(\hat{t}_j(\mathbf{x}_i))$. Here, $\hat{t}_j(\mathbf{x}_i)$ refers to the text prompt corresponding to the j -th largest cosine similarity.

²In this paper, $\mathbf{z}_I(\mathbf{x}_i)$ and $\mathbf{z}_T(t_j)$ are normalized features

3.1 Δ Energy for OOD detection

The proposed Δ Energy, which measures the energy change after modifying the top- c maximum cosine similarities³, unfolds as follows:

- Based on a pre-trained VLM, for each image feature $\mathbf{z}_I(\mathbf{x}_i)$, we first select the text feature sets $\{\mathbf{h}_j(\mathbf{x}_i)\}_{j=1}^c$ that have the top c similarity with $\mathbf{z}_I(\mathbf{x}_i)$.
- We then compute the product between each image feature $\mathbf{z}_I(\mathbf{x}_i)$ and the selected text feature $\mathbf{h}_j(\mathbf{x}_i)$. The product feature is represented as $\mathbf{z}_P(\mathbf{x}_i, \hat{t}_j) = \mathbf{z}_I(\mathbf{x}_i) \odot \mathbf{h}_j(\mathbf{x}_i)$.
- For each text feature $\mathbf{h}_j(\mathbf{x}_i)$ ($j \in [1, \dots, c]$), we denote the j -th largest cosine similarity between the image feature and the text feature as $s_{\hat{y}_j}(\mathbf{x}_i) = \mathbf{z}_I(\mathbf{x}_i) \cdot \mathbf{h}_j(\mathbf{x}_i)$. Let $\tilde{s}_{\hat{y}_j}(\mathbf{x}_i)$ represents the new cosine similarity after re-alignment, which is achieved by:

$$\tilde{s}_{\hat{y}_j}(\mathbf{x}_i) = 0 \quad (1)$$

- Finally, we can compute the new OOD score as: $\Delta\text{Energy}(\mathbf{x}_i) = E_1(\mathbf{x}_i) - E_0(\mathbf{x}_i)$. Based on the scaling temperature τ , $E_0(\mathbf{x}_i)$ is the energy score before the re-alignment:

$$E_0(\mathbf{x}_i) = -\log \sum_{j=1}^K e^{s_j(\mathbf{x}_i)/\tau} \quad (2)$$

$E_1(\mathbf{x}_i)$ is the energy score after the re-alignment:

$$E_1(\mathbf{x}_i) = -\frac{1}{c} \sum_{j=1}^c \log \left[e^{\tilde{s}_{\hat{y}_j}(\mathbf{x}_i)/\tau} + \sum_{p \neq \hat{y}_j} e^{s_p(\mathbf{x}_i)/\tau} \right] \quad (3)$$

We provide formal guarantees that the proposed Δ Energy can provably surpass the widely-used VLM-based OOD detection method MCM (Ming et al., 2022a).

Theorem 3.2. [OOD Detection Ability of Δ Energy] Suppose that the maximum cosine similarity for an ID sample \mathbf{x}_{ID} is greater than that of an open-set OOD sample \mathbf{x}_{OOD} , i.e., $s_{\hat{y}_1}(\mathbf{x}_{ID}) > s_{\hat{y}_1}(\mathbf{x}_{OOD})$. Let $S_{\text{Method}}(\mathbf{x})$ denote the score assigned to sample \mathbf{x} under a given method. We have the following properties: 1) $S_{\Delta\text{Energy}}(\mathbf{x}_{ID}) > S_{\Delta\text{Energy}}(\mathbf{x}_{OOD})$ for ID (\mathbf{x}_{ID}) and open-set OOD (\mathbf{x}_{OOD}) samples. 2) Compared to the MCM method, Δ Energy amplifies the difference between ID and OOD data, i.e., $d_{\Delta\text{Energy}} > d_{MCM}$, where $d_{\text{Method}} = S_{\text{Method}}(\mathbf{x}_{ID}) - S_{\text{Method}}(\mathbf{x}_{OOD})$.

Theorem 3.3. [The proposed OOD Score Δ Energy gets lower FPR than MCM] Given a task with closed-set ID label set $\mathcal{Y}_{\text{in}} = \{y_1, y_2, \dots, y_K\}$ and a pre-trained VLM, for any test input \mathbf{x}' , based on the scaling temperature τ , the maximum concept matching (MCM) score is computed as follows:

$$S_{\text{MCM}}(\mathbf{x}'; \mathcal{Y}_{\text{in}}) = \max_i \frac{e^{s_i(\mathbf{x}')/\tau}}{\sum_{j=1}^K e^{s_j(\mathbf{x}')/\tau}}.$$

For any $c \in \{1, 2, \dots, K\}$, if $s_{\hat{y}_1}(\mathbf{x}') \leq \tau \ln 2$, we have

$$\text{FPR}^{\Delta\text{Energy}}(\tau, \lambda) \leq \text{FPR}^{\text{MCM}}(\tau, \lambda),$$

where $\text{FPR}^{\Delta\text{Energy}}(\tau, \lambda)$ and $\text{FPR}^{\text{MCM}}(\tau, \lambda)$ is the false positive rate of Δ Energy and MCM, respectively, based on the temperature τ and detection threshold λ .

3.2 The Δ Energy-based bound maximization enhances OOD detection and generalization

Furthermore, as illustrated in Equation 6, we introduce a Δ Energy-based bound maximization function (EBM) during the fine-tuning process, which aims at increasing the lower bound of Δ Energy score for closed-set classes as demonstrated in Theorem 3.4. As illustrated in Theorem 3.5, the proposed objective function is theoretically proven to not only improve OOD detection but also lead to a domain-consistent Hessian, which serves as a strong indicator of OOD generalization.

³To enlarge the energy change for closed-set data, we perform re-alignment based on the top- c similarities.

Specifically, motivated by further enlarging ΔEnergy , we propose to minimize the following term:

$$\mathcal{L}_{\Delta E} = \frac{1}{N} \sum_{i=1}^N [E_2(\mathbf{x}_i) - E_0(\mathbf{x}_i)] \quad (4)$$

where N is the number of few-shot ID samples during fine-tuning and $E_2(\mathbf{x}_i)$ is the energy score for \mathbf{x}_i after masking on the image feature, which is formally calculated as:

$$E_2(\mathbf{x}_i) = -\log \sum_{j=1}^K e^{s'_j(\mathbf{x}_i)/\tau} \quad (5)$$

$$s'_j(\mathbf{x}_i) = (\mathbf{z}_I(\mathbf{x}_i) \odot \mathbf{m}'(\mathbf{x}_i)) \cdot \mathbf{z}_T(t_j) \quad (6)$$

Here, $\mathbf{m}'(\mathbf{x}_i)$ is the mask that retains the top p -proportion elements in $\mathbf{z}_I(\mathbf{x}_i) \odot \mathbf{h}_1(\mathbf{x}_i)$ and $\mathbf{h}_1(\mathbf{x}_i)$ is the text feature corresponding to the top-1 cosine similarity.

Theorem 3.4. *[EBM increase the lower bound of ΔEnergy]* Let $\mathbf{h}_1(\mathbf{x}_i)$ denote the text feature that have the top-1 similarity with the image feature $\mathbf{z}_I(\mathbf{x}_i)$. The corresponding similarity is computed as $s_{\hat{y}_1}(\mathbf{x}_i) = \mathbf{z}_I(\mathbf{x}_i) \cdot \mathbf{h}_1(\mathbf{x}_i)$. Suppose that $\mathcal{L}_{\Delta E} \leq \varepsilon_E$, with $c = 1$, under the condition that:

$$\sum_{i=1}^N e^{s_{\hat{y}_1}(\mathbf{x}_i)/\tau} - e^{\tilde{s}_{\hat{y}_1}(\mathbf{x}_i)/\tau} \geq \sum_{i=1}^N (e^{\varepsilon_E} - 1) e^{-E_2(\mathbf{x}_i)} \quad (7)$$

we have $\frac{1}{N} \sum_{i=1}^N \Delta\text{Energy}(\mathbf{x}_i) \geq -\mathcal{L}_{\Delta E}$.

Theorem 3.4 implies that if the change in the VLM's predictions after re-alignment is not too small and satisfies the condition as shown in Equation 7, minimizing $\mathcal{L}_{\Delta E}$ can increase the lower bound of ΔEnergy for closed-set classes. Moreover, we theoretically demonstrated that the proposed EBM loss in Equation 6 can also lead to domain-consistent Hessians of classification loss, which serves as a strong indicator for OOD generalization (Rame et al., 2022; Hemati et al., 2023).

Theorem 3.5. *[EBM leads to domain-consistent Hessians]* Given the ID training data sampled from domain \mathcal{S} and the learnable parameter θ in VLM, we denote the masked domain as \mathcal{S}' . We represent the empirical classification loss on the domain \mathcal{D} as $\hat{\mathcal{E}}_{\mathcal{D}}(\theta)$. Let $\hat{\mathbf{G}}_{\mathcal{D}}(\theta)$ and $\hat{\mathbf{H}}_{\mathcal{D}}(\theta)$ be the gradient vector and Hessian matrix of empirical risk $\hat{\mathcal{E}}_{\mathcal{D}}(\theta)$ over parameter θ , respectively. In this paper, we propose to minimize $\mathcal{L}_{\Delta E}$. The distance between the unmasked and masked image feature is assumed to satisfy: $\|\mathbf{z}_I(\mathbf{x}_i) - (\mathbf{z}_I(\mathbf{x}_i) \odot \mathbf{m}'(\mathbf{x}_i))\|_2 \leq \varepsilon$. Then the local optimum θ of $\min \mathcal{L}_{\Delta E}$ satisfies:

$$|\theta^\top (\hat{\mathbf{H}}_{\mathcal{S}}(\theta) - \hat{\mathbf{H}}_{\mathcal{S}'}(\theta))\theta| \leq \frac{\varepsilon}{N} \sum_{i=1}^N |\theta^\top \nabla_{\theta}^2 \mathbf{z}_T(\mathbf{x}_i)\theta|$$

Proposition 3.6. *[EBM bound OOD generalization]* Let $\mathbf{z}_I(\mathbf{x}_i)$ and $\tilde{\mathbf{z}}_I(\mathbf{x}_i)$ denote the image feature from source domain (\mathcal{S}) and target domain (\mathcal{T}), respectively. We assume that $\|\mathbf{z}_I(\mathbf{x}_i) - \tilde{\mathbf{z}}_I(\mathbf{x}_i)\|_2 \leq \varepsilon_1$. By applying the second-order Taylor expansion and utilizing the domain-consistent Hessians as outlined in Theorem 3.5, the OOD generalization gap between source domain (\mathcal{S}) and target domain (\mathcal{T}) is upper bounded by the following inequality:

$$\max_{\{\theta: |\hat{\mathcal{E}}_{\mathcal{S}}(\theta) - \hat{\mathcal{E}}_{\mathcal{S}}(\theta^*)| \leq \varepsilon\}} |\hat{\mathcal{E}}_{\mathcal{T}}(\theta) - \hat{\mathcal{E}}_{\mathcal{S}}(\theta^*)| \lesssim |\hat{\mathcal{E}}_{\mathcal{T}}(\theta^*) - \hat{\mathcal{E}}_{\mathcal{S}}(\theta^*)| + \max \frac{1}{2} |\theta^\top \hat{\mathbf{H}}_{\mathcal{S}}(\theta^*)\theta| + O(\varepsilon_1)$$

where θ^* is a local minimum across all domains, i.e., $\nabla_{\theta} \hat{\mathcal{E}}_{\mathcal{D}}(\theta^*) = \mathbf{0}$.

Therefore, by connecting the EBM loss with the Hessians of empirical classification loss, we theoretically discover that the EBM loss can lead to a bound of the performance gap between closed-set ID data and closed-set OOD data. This implies that optimizing for ΔEnergy with EBM loss also involves optimizing for OOD generalization.

Table 1: **OOD detection between closed-set data and open-set OOD data based on ImageNet-1k:** OOD detection measured by AUROC and FPR95 over the mixture of closed-set test sets and open-set OOD test sets.

DATA	Method	Energy	ODIN	ReAct	CLIPN	MSP	MaxLogit	MCM	NegLabel	CSP	$\Delta E_{\text{Energy}} (\text{Ours})$
ID vs.	FPR95 \downarrow	76.72	51.71	80.38	64.37	51.72	69.12	53.34	77.31	68.49	46.40 (2.58)
Semantic-shifted OOD	AUROC \uparrow	76.94	85.61	74.06	81.44	85.64	80.28	85.81	75.73	78.84	87.10 (0.75)
Covariate-shifted OOD vs.	FPR95 \downarrow	83.94	61.25	85.05	84.44	69.20	79.80	70.30	82.81	79.76	67.16 (0.38)
Semantic-shifted OOD	AUROC \uparrow	67.21	77.10	64.66	64.64	78.64	70.52	75.66	67.38	67.89	78.68 (0.57)

Table 2: **OOD detection between closed-set data and open-set OOD data based on PACS and VLCS:** OOD detection measured by AUROC and FPR95 over the mixture of closed-set OOD and open-set OOD test sets.

DATA	PACS vs. Open-Set (AUC \uparrow / FPR95 \downarrow)			VLCS vs. Open-Set (AUC \uparrow / FPR95 \downarrow)			AVG
	Method	DTD	Food101	Caltech101	DTD	Food101	Caltech101
Energy	82.4 / 67.6	95.9 / 26.0	86.7 / 52.2	55.3 / 88.8	85.8 / 48.3	53.3 / 86.3	76.6 / 61.5
ReAct	89.5 / 44.9	98.1 / 9.9	89.8 / 43.2	52.8 / 89.7	86.7 / 47.8	61.4 / 83.2	79.7 / 53.1
CLIPN	93.6 / 40.3	96.2 / 25.6	88.1 / 56.1	80.4 / 62.7	88.9 / 46.6	72.5 / 74.1	86.6 / 50.9
MaxLogit	89.5 / 45.1	97.9 / 13.1	88.9 / 46.8	60.8 / 87.6	88.9 / 45.4	69.4 / 81.6	82.6 / 53.3
MSP	97.9 / 9.8	98.9 / 4.6	95.8 / 20.9	84.4 / 55.3	93.7 / 35.1	88.9 / 48.8	93.3 / 29.1
ODIN	99.1 / 1.8	99.3 / 1.0	97.4 / 6.7	83.1 / 46.5	91.3 / 28.2	86.8 / 40.9	92.8 / 17.9
MCM	98.9 / 4.3	99.2 / 3.4	97.0 / 13.7	84.2 / 55.1	93.3 / 36.4	88.5 / 50.4	93.5 / 27.2
NegLabel	99.3 / 4.2	97.7 / 15.8	95.7 / 31.6	84.8 / 54.3	79.4 / 74.6	62.7 / 84.3	86.6 / 49.1
CSP	99.6 / 1.8	99.2 / 2.6	97.8 / 12.4	88.9 / 38.7	78.3 / 67.4	67.3 / 73.0	88.5 / 32.7
$\Delta E_{\text{Energy}} (\text{Ours})$	98.1 / 6.5	99.2 / 2.4	96.1 / 14.3	85.3 / 53.2	94.1 / 31.9	89.5 / 47.3	93.7 / 25.9

3.3 Overview of the proposed method

Our theoretical analysis thus leads to the design of a new fine-tuning framework with concurrent optimization for both tasks. As illustrated in Figure 2, we prioritize computational efficiency by adopting prompt-tuning techniques. In the fine-tuning process, both the image encoder and text encoder are frozen and only the context vectors θ are learnable. Let \mathcal{L}_{CE} denote the Cross-Entropy loss and λ_0 denote the hyperparameter that can be chosen based on the validation procedure. Then the final optimization objective of the EBM method is expressed as:

$$\mathcal{L}_{\text{EBM}} = \mathcal{L}_{\text{CE}} + \lambda_0 e^{\mathcal{L}_{\Delta E}} \quad (8)$$

4 Experiments

In this section, motivated by the remarkable success of the vision-language model CLIP (Radford et al., 2021) in learning general visual knowledge, we conduct experiments based on CLIP. First, we conduct extensive experiments to validate the effectiveness of the proposed ΔE_{Energy} in zero-shot OOD detection across various datasets. Furthermore, we evaluate the effect of the proposed EBM method in enhancing both OOD generalization and OOD detection. Due to space limitations, we provide ablation studies in Appendix G to validate our theoretical findings.

4.1 Effectiveness of ΔE_{Energy} for OOD detection

Dataset We evaluate OOD detection performance over 4 different benchmarks, including 1) the discrimination between closed-set OOD data and open-set OOD data based on ImageNet-1k, 2) the discrimination between closed-set OOD data and open-set OOD data based on cross-dataset images, 3) hard OOD detection on different splits of ImageNet-1k, 4) the conventional OOD detection benchmark. For the first two benchmark datasets, we evaluate the models’ OOD detection capabilities under more challenging scenarios, where the datasets exhibit both covariate and semantic shifts. Models are required to distinguish between various types of closed-set OOD data (covariate shifts) and open-set OOD data (semantic shifts). Details of the two data settings are illustrated as follows:

1) *Setup-I: open-set discrimination on the large-scale ImageNet-1k dataset.* Following the prior work (Zhu et al., 2024), we split ImageNet-1k (Krizhevsky et al., 2017) into open and closed sets w.r.t class labels. We randomly define 40% classes of ImageNet as the closed-set, and the remaining 60% as the open-set. The samples from ImageNet-A (Hendrycks et al., 2021b), ImageNet-R (Hendrycks et al., 2021a), ImageNet-Sketch (Wang et al., 2019), and ImageNet-V2 (Recht et al., 2019), which share the same class labels as the closed-set ID data, are considered as closed-set OOD data.

2) *Setup-II: open-set discrimination on cross-dataset images.* Using cross-dataset examples as the open-set is another established protocol (Shafaei et al., 2018; Kong and Ramanan, 2021). Following

Table 3: **Tuning-based results on Setup-I:** Comparison with competitive fine-tuning methods based on CLIP ViT-B/16 using 16 samples per class. In the testing phase of LoCoOp, NegPrompt and GalLoP, we use the GL-MCM score (Miyai et al., 2023) to compute OOD detection results.

Algorithm OOD Score	CoOp MCM	CoCoOp MCM	CLIP-Adapter MCM	Bayes-CAL MCM	DPLCLIP MCM	CRoFT MCM	LoCoOp GL	NegPrompt GL	GalLoP GL	EBM (Ours) ΔEnergy
ID ACC \uparrow	82.11	81.59	79.91	82.31	82.46	82.03	82.14	81.46	84.51	81.52 (0.4)
OOD ACC \uparrow	61.36	62.58	60.58	61.95	61.53	62.83	61.18	60.39	61.75	63.28 (0.2)
AUROC \uparrow	72.94	76.38	74.86	74.44	72.81	76.30	70.03	60.86	56.97	81.90 (1.9)
FPR95 \downarrow	73.15	70.30	70.92	72.34	73.07	69.78	74.33	86.66	91.17	65.90 (1.7)

the prior work (Gulrajani and Lopez-Paz, 2021; Cha et al., 2022; Ye et al., 2021), we leverage popular datasets like PACS (Li et al., 2017) or VLCS (Li et al., 2017) for domain generalization studies as the closed-set data. We evaluate the models’ ability to distinguish between closed-set OOD and cross-dataset images by utilizing different styles of datasets like Caltech101 (Bansal et al., 2021), DTD (Sharan et al., 2014), and Food101 (Bossard et al., 2014) as open-set OOD examples. All overlapping classes are removed from the three open-set OOD datasets.

In addressing the hard OOD detection scenarios, we follow the prior works (Ming et al., 2022a; Li et al., 2024a; Chen et al., 2024) and partition the ImageNet1k dataset into two parts: one part of the data serves as the ID, while the other serves as OOD. For conventional OOD detection, we use a popular benchmark in which ImageNet-1k (Krizhevsky et al., 2017) with 1,000 classes is used as the ID dataset, and the OOD datasets including subsets of Texture (Cimpoi et al., 2014), iNaturalist (Van Horn et al., 2018), Places (Zhou et al., 2017) and SUN (Xiao et al., 2010).

Comparison methods To substantiate the effectiveness of the proposed OOD score, we conduct an empirical analysis of distinct categories of methodologies for OOD detection utilizing VLMs. These categories encompass zero-shot approaches and the methods that combine the CLIP image encoder with classical approaches. For zero-shot methods, we opted for 4 recent methods, MCM (Ming et al., 2022a), CLIPN (Wang et al., 2023a), NegLabel (Jiang et al., 2024) and CSP (Chen et al., 2024). MCM employs the original CLIP, utilizing the maximum softmax probability operation on the similarities for detection, and CLIPN involves an additional training phase during pre-training, specifically training a negative text encoder using large external data. Both the NegLabel and CSP methods introduce additional negative labels, enabling more accurate OOD detection. For the second group of methods, we adapt previous logits-based methodologies to the use of the CLIP image encoder, including MSP (Hendrycks and Gimpel, 2016), Energy (Liu et al., 2020), MaxLogit (Hendrycks et al., 2019), ReAct (Sun et al., 2021) and ODIN (Liang et al., 2017a). Following the previous studies (Wang et al., 2023a), we use CLIP based on ViT-B/16, which is pre-trained from OpenCLIP.

Metrics Two OOD detection metrics are used. The first is the False Positive Rate at a 95% True Negative Rate (FPR95), which denotes the rate of falsely identified OOD instances when the true negative rate is maintained at 95%. The second is the Area Under the Receiver Operating Characteristic curve (AUROC), representing the measure of OOD ranking across various classification thresholds.

Experiments results For zero-shot OOD detection, we set $c = 2$ and $\tau = 0.01$ in our ΔEnergy . We present the results of ΔEnergy and competitors in discriminating between closed-set data and open-set OOD data in Table 1-2. Due to space limitations, we provide the results on the traditional OOD detection and hard OOD detection datasets in Table 5-7 in Appendix G. It is observed that the proposed ΔEnergy obtains the top-1 AUROC performance on all benchmarks. Compared with the vanilla energy-based OOD detection method (Liu et al., 2020), our ΔEnergy method consistently achieves better OOD detection performance across all 4 benchmarks. Notably, as shown in Table 1–2, our approach surpasses the competitive NegLabel and CSP methods by a large margin, demonstrating the superiority of the proposed method in distinguishing different semantics in open-world scenarios. The inferior performances of NegLabel and CSP may stem from the underlying assumption of these methods—that OOD samples possess a variety of distinct visual properties—which may not hold in hard OOD detection scenarios where OOD samples are distributed closely with closed-set data. Furthermore, the presence of covariate shifts reduces the similarity between closed-set OOD and ID data, thereby making it more difficult to distinguish closed-set OOD data from open-set OOD data.

4.2 Effectiveness of the EBM loss for both OOD generalization and OOD detection

Datasets To substantiate the effectiveness of the proposed EBM method for both tasks, we evaluate our method under two data settings (Setup-I and Setup-II), each incorporating both covariate shifts and semantic shifts, as introduced in Section 4.1. For evaluating OOD generalization performance on

Table 4: **Tuning-based results on Setup-II:** Comparison with competitive fine-tuning methods based on CLIP ViT-B/16 using 16 samples per class.

DATA	PACS OOD ACC \uparrow	PACS vs. Open-Set (AUROC \uparrow / FPR95 \downarrow)			VLCS OOD ACC \uparrow	VLCS vs. Open-Set (AUROC \uparrow / FPR95 \downarrow)			AVG FPR \downarrow
		DTD	Food101	Caltech101		DTD	Food101	Caltech101	
ZS CLIP+ MCM	96.1 (0.0)	98.9 / 4.3	99.2 / 3.4	97.0 / 13.7	75.1 (0.0)	84.2 / 55.1	93.3 / 36.4	88.5 / 50.4	27.2
ZS CLIP + Δ Energy	96.1 (0.0)	98.1 / 6.5	99.2 / 2.4	96.1 / 14.3	75.1 (0.0)	85.3 / 53.2	94.1 / 29.7	89.5 / 47.3	25.5
CoOp	96.3 (0.7)	98.9 / 4.6	99.2 / 3.1	97.4 / 11.2	78.3 (1.7)	89.3 / 37.6	91.4 / 40.1	85.9 / 47.4	24.0
CoCoOp	96.8 (0.5)	98.8 / 4.0	98.7 / 5.8	97.5 / 10.9	78.9 (0.8)	88.3 / 44.9	89.2 / 44.6	86.8 / 48.6	26.5
CLIP-Adapter	96.1 (0.0)	99.0 / 4.1	99.2 / 3.6	97.4 / 12.1	77.3 (0.7)	85.9 / 52.4	93.8 / 35.5	89.3 / 48.5	26.0
Bayes-CAL	96.6 (0.5)	98.5 / 7.2	98.3 / 8.8	95.9 / 16.6	79.6 (0.9)	88.0 / 47.7	84.9 / 61.1	84.8 / 56.7	33.0
DPLCLIP	95.6 (0.2)	96.6 / 21.6	97.1 / 18.1	92.2 / 35.1	76.5 (1.3)	88.9 / 37.1	86.8 / 43.2	84.2 / 50.2	34.2
LoCoOp	96.5 (0.3)	98.1 / 9.7	98.4 / 8.6	95.9 / 19.4	76.3 (0.7)	86.1 / 50.9	84.3 / 62.8	83.3 / 59.7	35.2
GalLoP	96.9 (0.2)	98.6 / 5.6	98.3 / 8.9	95.4 / 18.2	81.3 (0.9)	87.4 / 39.0	91.0 / 43.4	80.7 / 59.1	29.0
CRoFT	97.3 (0.1)	94.0 / 33.0	89.9 / 57.7	84.0 / 71.2	80.2 (1.0)	90.2 / 40.6	80.1 / 70.3	79.0 / 66.4	56.5
NegPrompt	97.1 (0.4)	88.9 / 42.2	97.5 / 15.2	94.4 / 22.6	77.8 (0.6)	93.4 / 29.6	89.8 / 39.6	75.2 / 72.4	36.9
EBM + MCM	<u>97.2 (0.1)</u>	<u>98.6 / 5.6</u>	<u>99.0 / 4.3</u>	<u>96.8 / 13.7</u>	81.7 (0.6)	<u>91.6 / 32.6</u>	<u>93.3 / 32.7</u>	<u>86.5 / 44.1</u>	<u>22.2</u>
EBM + Δ Energy	<u>97.2 (0.1)</u>	<u>98.2 / 6.3</u>	<u>98.7 / 3.8</u>	<u>96.6 / 14.8</u>	81.7 (0.6)	<u>91.7 / 30.2</u>	<u>93.6 / 28.6</u>	<u>86.4 / 42.5</u>	21.0

Setup-II, we utilize the leave-one-domain-out validation protocol (Gulrajani and Lopez-Paz, 2020) that uses three domains as closed-set ID data and the remaining one as closed-set OOD data.

Comparison methods We conduct an empirical analysis of distinct categories of CLIP-based lightweight fine-tuning methods. In addition to comparing our approach with popular fine-tuning techniques, such as the widely-used CoOp (Zhou et al., 2021), CoCoOp (Zhou et al., 2022) and CLIP-Adapter (Gao et al., 2023), we also evaluate it against CLIP-based methods designed specifically for OOD generalization or OOD detection. For OOD generalization, we compare our EBM with methods like DPLCLIP (Zhang et al., 2021b) and Bayes-CAL (Zhu et al., 2023b, 2025b). For OOD detection, we consider approaches such as LoCoOp (Miyai et al., 2024b), NegPrompt (Li et al., 2024a), CRoFT (Zhu et al., 2024), and GalLoP (Lafon et al., 2024), with CRoFT and GalLoP explicitly designed to optimize both OOD generalization and detection.

Experiment details We conduct experiments based on the CLIP ViT-B/16 model using 16 samples per ID classes. For the prompt learning methods, we use random initialization for context vectors and set the number of context tokens to 16. Without otherwise specified, methods are trained using the SGD optimizer with a learning rate of 0.002 and batch size of 32 for fair comparisons. We set the maximum training epoch to 30 for all models. For all baseline methods, we follow the hyperparameter searching protocols recommended in their original papers. For our EBM method, we search for λ_0 in [0.1, 0.5, 1.0] for Setup-I and we set $\lambda_0 = 2$ for Setup-II. We set $\tau = 0.01$ and $c = 2$ in Δ Energy, and we vary the masking proportion $p\%$ within the range of [0.4, 0.5, 0.6] in $\mathcal{L}_{\Delta E}$. For experiments on each method, we repeat 3 times with different random splits to eliminate the effects of randomness. Finally, we report the average classification accuracy on closed-set test sets, as well as the average FPR95 and AUROC results for distinguishing between open-set OOD data and closed-set OOD data based on MCM (GL-MCM) (Ming et al., 2022a; Miyai et al., 2023) or our Δ Energy.

Experiment results We present the results of setup-I in Table 3, where the proposed EBM method establishes the overall best performance in both OOD generalization and OOD detection. Notably, our method outperforms the competitive CRoFT (Zhu et al., 2024) method, which is introduced to achieve concurrent optimization on both tasks. Our method obtains a 0.45% improvement on OOD accuracy in closed-set OOD data and more than 5% improvements on AUROC when discriminating closed-set OOD datasets and open-set OOD classes. In contrast, although the competitors can achieve higher ID test accuracy, they often struggle with the OOD generalization or OOD detection task, even resulting in worse performance when compared to the zero-shot CLIP model. Moreover, it is observed that recent methods, such as GalLoP (Lafon et al., 2024) and NegPrompt (Li et al., 2024a), aimed at improving VLMs’ OOD detection may not scale well to handling different types of distribution shifts in large-scale ImageNet-1k datasets. The results of setup-II are shown in Table 4, where the EBM method also demonstrates the best overall performance on both tasks. Consistent with the results of Setup-I, its competitors, especially those (Zhu et al., 2023b; Zhang et al., 2021b; Zhu et al., 2024) designed for OOD generalization, achieve even higher FPR95 scores compared to the CLIP model. Notably, for the more challenging VLCS dataset, our EBM method shows significant performance improvements over CRoFT and GalLoP on both tasks. This is likely due to the fact that CRoFT performs adapter-tuning on both the image and text inputs, which can lead to forgetting the general knowledge encoded in the pre-trained CLIP model. In contrast, based on fine-tuning language model, our method optimizes the energy change when re-aligning vision-language modalities, resulting in more robust performance across various datasets. These results highlight the EBM method’s ability to more effectively enhance both OOD generalization and OOD detection.

5 Conclusions

Different from the vanilla energy-based OOD score, we propose a novel zero-shot OOD detection method, Δ Energy, which measures the energy change when re-aligning vision-language modalities. Both theoretical and experimental results demonstrate that Δ Energy provides more reliable OOD detection than previous methods. Furthermore, we introduce a Δ Energy-based bound maximization during fine-tuning VLMs. The proposed bound maximization is theoretically proven to not only improve OOD detection but also lead to optimization for OOD generalization. Building on this insight, we have developed a unified fine-tuning framework that enables the concurrent optimization of both tasks. Extensive experiments on challenging OOD detection and generalization benchmarks demonstrate the superiority of our method.

Acknowledgements

This work is supported by National Natural Science Foundation of China (No.62572313, No.62106139).

References

- Haoyue Bai, Gregory Canal, Xuefeng Du, Jeongyeol Kwon, Robert D Nowak, and Yixuan Li. Feed two birds with one scone: Exploiting wild data for both out-of-distribution generalization and detection. In *International Conference on Machine Learning*, pages 1454–1471. PMLR, 2023.
- Yichen Bai, Zongbo Han, Bing Cao, Xiaoheng Jiang, Qinghua Hu, and Changqing Zhang. Id-like prompt learning for few-shot out-of-distribution detection. In *Proceedings of the IEEE/CVF Conference on Computer Vision and Pattern Recognition*, pages 17480–17489, 2024.
- Monika Bansal, Munish Kumar, Monika Sachdeva, and Ajay Mittal. Transfer learning for image classification using vgg19: Caltech-101 image data set. *Journal of ambient intelligence and humanized computing*, pages 1–12, 2021.
- Hangbo Bao, Wenhui Wang, Li Dong, Qiang Liu, Owais Khan Mohammed, Kriti Aggarwal, Subhajit Som, Songhao Piao, and Furu Wei. Vlmo: Unified vision-language pre-training with mixture-of-modality-experts. *Advances in Neural Information Processing Systems*, 35:32897–32912, 2022.
- Petra Bevandić, Ivan Krešo, Marin Oršić, and Siniša Šegvić. Dense outlier detection and open-set recognition based on training with noisy negative images. *arXiv preprint arXiv:2101.09193*, 2021.
- Lukas Bossard, Matthieu Guillaumin, and Luc Van Gool. Food-101–mining discriminative components with random forests. In *Computer Vision–ECCV 2014: 13th European Conference, Zurich, Switzerland, September 6–12, 2014, Proceedings, Part VI 13*, pages 446–461. Springer, 2014.
- Junbum Cha, Kyungjae Lee, Sungrae Park, and Sanghyuk Chun. Domain generalization by mutual-information regularization with pre-trained models. In *European Conference on Computer Vision*, pages 440–457. Springer, 2022.
- Mengyuan Chen, Junyu Gao, and Changsheng Xu. Conjugated semantic pool improves ood detection with pre-trained vision-language models. *arXiv preprint arXiv:2410.08611*, 2024.
- Mircea Cimpoi, Subhransu Maji, Iasonas Kokkinos, Sammy Mohamed, and Andrea Vedaldi. Describing textures in the wild. In *Proceedings of the IEEE conference on computer vision and pattern recognition*, pages 3606–3613, 2014.
- Xuefeng Du, Gabriel Gozum, Yifei Ming, and Yixuan Li. Siren: Shaping representations for detecting out-of-distribution objects. *Advances in Neural Information Processing Systems*, 35:20434–20449, 2022a.
- Xuefeng Du, Zhaoning Wang, Mu Cai, and Yixuan Li. Vos: Learning what you don’t know by virtual outlier synthesis. *arXiv preprint arXiv:2202.01197*, 2022b.

- Yarin Gal and Zoubin Ghahramani. Dropout as a bayesian approximation: Representing model uncertainty in deep learning. In *international conference on machine learning*, pages 1050–1059. PMLR, 2016.
- Peng Gao, Shijie Geng, Renrui Zhang, Teli Ma, Rongyao Fang, Yongfeng Zhang, Hongsheng Li, and Yu Qiao. Clip-adapter: Better vision-language models with feature adapters. *International Journal of Computer Vision*, pages 1–15, 2023.
- Chuanxing Geng, Sheng-jun Huang, and Songcan Chen. Recent advances in open set recognition: A survey. *IEEE transactions on pattern analysis and machine intelligence*, 43(10):3614–3631, 2020.
- Muhammad Waleed Gondal, Jochen Gast, Inigo Alonso Ruiz, Richard Droste, Tommaso Macri, Suren Kumar, and Luitpold Staudigl. Domain aligned clip for few-shot classification. In *Proceedings of the IEEE/CVF Winter Conference on Applications of Computer Vision*, pages 5721–5730, 2024.
- Koustava Goswami, Srikrishna Karanam, Prateksha Udhayanan, KJ Joseph, and Balaji Vasan Srinivasan. Copl: Contextual prompt learning for vision-language understanding. In *Proceedings of the AAAI Conference on Artificial Intelligence*, pages 18090–18098, 2024.
- Sachin Goyal, Ananya Kumar, Sankalp Garg, Zico Kolter, and Aditi Raghunathan. Finetune like you pretrain: Improved finetuning of zero-shot vision models. In *Proceedings of the IEEE/CVF Conference on Computer Vision and Pattern Recognition*, pages 19338–19347, 2023.
- Ishaan Gulrajani and David Lopez-Paz. In search of lost domain generalization. *arXiv preprint arXiv:2007.01434*, 2020.
- Ishaan Gulrajani and David Lopez-Paz. In search of lost domain generalization. In *ICLR*, 2021.
- Sobhan Hemati, Guojun Zhang, Amir Estiri, and Xi Chen. Understanding hessian alignment for domain generalization. In *Proceedings of the IEEE/CVF International Conference on Computer Vision*, pages 19004–19014, 2023.
- Dan Hendrycks and Kevin Gimpel. A baseline for detecting misclassified and out-of-distribution examples in neural networks. *arXiv preprint arXiv:1610.02136*, 2016.
- Dan Hendrycks, Steven Basart, Mantas Mazeika, Andy Zou, Joe Kwon, Mohammadreza Mostajabi, Jacob Steinhardt, and Dawn Song. Scaling out-of-distribution detection for real-world settings. *arXiv preprint arXiv:1911.11132*, 2019.
- Dan Hendrycks, Steven Basart, Norman Mu, Saurav Kadavath, Frank Wang, Evan Dorundo, Rahul Desai, Tyler Zhu, Samyak Parajuli, Mike Guo, et al. The many faces of robustness: A critical analysis of out-of-distribution generalization. In *Proceedings of the IEEE/CVF International Conference on Computer Vision*, pages 8340–8349, 2021a.
- Dan Hendrycks, Kevin Zhao, Steven Basart, Jacob Steinhardt, and Dawn Song. Natural adversarial examples. In *Proceedings of the IEEE/CVF Conference on Computer Vision and Pattern Recognition*, pages 15262–15271, 2021b.
- Chen Huang, Skyler Seto, Samira Abnar, David Grangier, Navdeep Jaitly, and Josh Susskind. Aggregate-and-adapt natural language prompts for downstream generalization of clip. *arXiv preprint arXiv:2410.23698*, 2024.
- Tony Huang, Jack Chu, and Fangyun Wei. Unsupervised prompt learning for vision-language models. *arXiv preprint arXiv:2204.03649*, 2022.
- Jingjing Jiang, Ziyi Liu, and Nanning Zheng. Correlation information bottleneck: Towards adapting pretrained multimodal models for robust visual question answering, 2023.
- Xue Jiang, Feng Liu, Zhen Fang, Hong Chen, Tongliang Liu, Feng Zheng, and Bo Han. Negative label guided ood detection with pretrained vision-language models. *arXiv preprint arXiv:2403.20078*, 2024.
- Muhammad Uzair Khattak, Hanoona Rasheed, Muhammad Maaz, Salman Khan, and Fahad Shahbaz Khan. Maple: Multi-modal prompt learning. In *Proceedings of the IEEE/CVF Conference on Computer Vision and Pattern Recognition*, pages 19113–19122, 2023a.

Muhammad Uzair Khattak, Syed Talal Wasim, Muzammal Naseer, Salman Khan, Ming-Hsuan Yang, and Fahad Shahbaz Khan. Self-regulating prompts: Foundational model adaptation without forgetting. In *Proceedings of the IEEE/CVF International Conference on Computer Vision*, pages 15190–15200, 2023b.

Pang Wei Koh, Shiori Sagawa, Henrik Marklund, Sang Michael Xie, Marvin Zhang, Akshay Bal-subramani, Weihua Hu, Michihiro Yasunaga, Richard Lanas Phillips, Sara Beery, et al. Wilds: A benchmark of in-the-wild distribution shifts. *arXiv:2012.07421*, 2020.

Shu Kong and Deva Ramanan. Opengan: Open-set recognition via open data generation. In *Proceedings of the IEEE/CVF International Conference on Computer Vision*, pages 813–822, 2021.

Alex Krizhevsky, Ilya Sutskever, and Geoffrey E Hinton. Imagenet classification with deep convolutional neural networks. *Communications of the ACM*, 60(6):84–90, 2017.

Marc Lafon, Elias Ramzi, Clément Rambour, Nicolas Audebert, and Nicolas Thome. Gallop: Learning global and local prompts for vision-language models. In *European Conference on Computer Vision*, pages 264–282. Springer, 2024.

Chaohua Li, Enhao Zhang, Chuanxing Geng, and Songcan Chen. Recent advances in out-of-distribution detection with clip-like models: A survey. *arXiv preprint arXiv:2505.02448*, 2025.

Da Li, Yongxin Yang, Yi-Zhe Song, and Timothy M Hospedales. Deeper, broader and artier domain generalization. In *Proceedings of the IEEE international conference on computer vision*, pages 5542–5550, 2017.

Tianqi Li, Guansong Pang, Xiao Bai, Wenjun Miao, and Jin Zheng. Learning transferable negative prompts for out-of-distribution detection. In *Proceedings of the IEEE/CVF Conference on Computer Vision and Pattern Recognition*, pages 17584–17594, 2024a.

Zheng Li, Xiang Li, Xinyi Fu, Xin Zhang, Weiqiang Wang, Shuo Chen, and Jian Yang. Promptkd: Unsupervised prompt distillation for vision-language models. In *Proceedings of the IEEE/CVF Conference on Computer Vision and Pattern Recognition*, pages 26617–26626, 2024b.

Shiyu Liang, Yixuan Li, and Rayadurgam Srikant. Enhancing the reliability of out-of-distribution image detection in neural networks. *arXiv preprint arXiv:1706.02690*, 2017a.

Shiyu Liang, Yixuan Li, and Rayadurgam Srikant. Enhancing the reliability of out-of-distribution image detection in neural networks. *arXiv preprint arXiv:1706.02690*, 2017b.

Weitang Liu, Xiaoyun Wang, John Owens, and Yixuan Li. Energy-based out-of-distribution detection. *Advances in neural information processing systems*, 33:21464–21475, 2020.

Andrey Malinin and Mark Gales. Predictive uncertainty estimation via prior networks. *Advances in neural information processing systems*, 31, 2018.

Nicolai Meinshausen and Peter Bühlmann. Maximin effects in inhomogeneous large-scale data. *The Annals of Statistics*, 43(4), 2015.

Yifei Ming and Yixuan Li. How does fine-tuning impact out-of-distribution detection for vision-language models? *International Journal of Computer Vision*, 132(2):596–609, 2024.

Yifei Ming, Ziyang Cai, Jiuxiang Gu, Yiyou Sun, Wei Li, and Yixuan Li. Delving into out-of-distribution detection with vision-language representations. *Advances in neural information processing systems*, 35:35087–35102, 2022a.

Yifei Ming, Ying Fan, and Yixuan Li. Poem: Out-of-distribution detection with posterior sampling. In *International Conference on Machine Learning*, pages 15650–15665. PMLR, 2022b.

Atsuyuki Miyai, Qing Yu, Go Irie, and Kiyoharu Aizawa. Zero-shot in-distribution detection in multi-object settings using vision-language foundation models. *arXiv preprint arXiv:2304.04521*, 2023.

- Atsuyuki Miyai, Jingkang Yang, Jingyang Zhang, Yifei Ming, Yueqian Lin, Qing Yu, Go Irie, Shafiq Joty, Yixuan Li, Hai Li, et al. Generalized out-of-distribution detection and beyond in vision language model era: A survey. *arXiv preprint arXiv:2407.21794*, 2024a.
- Atsuyuki Miyai, Qing Yu, Go Irie, and Kiyoharu Aizawa. Locoop: Few-shot out-of-distribution detection via prompt learning. *Advances in Neural Information Processing Systems*, 36, 2024b.
- Vivek Narayanaswamy, Yamen Mubarka, Rushil Anirudh, Deepta Rajan, and Jayaraman J. Thiagarajan. Exploring inlier and outlier specification for improved medical ood detection. In *Proceedings of the IEEE/CVF International Conference on Computer Vision (ICCV) Workshops*, pages 4589–4598, 2023.
- Jun Nie, Yonggang Zhang, Zhen Fang, Tongliang Liu, Bo Han, and Xinmei Tian. Out-of-distribution detection with negative prompts. In *The twelfth international conference on learning representations*, 2024.
- Stanislav Pidhorskyi, Ranya Almohsen, and Gianfranco Doretto. Generative probabilistic novelty detection with adversarial autoencoders. *Advances in neural information processing systems*, 31, 2018.
- Alec Radford, Jong Wook Kim, Chris Hallacy, Aditya Ramesh, Gabriel Goh, Sandhini Agarwal, Girish Sastry, Amanda Askell, Pamela Mishkin, Jack Clark, Gretchen Krueger, and Ilya Sutskever. Learning transferable visual models from natural language supervision. *CoRR*, abs/2103.00020, 2021.
- Alexandre Rame, Corentin Dancette, and Matthieu Cord. Fishr: Invariant gradient variances for out-of-distribution generalization. In *International Conference on Machine Learning*, pages 18347–18377. PMLR, 2022.
- Benjamin Recht, Rebecca Roelofs, Ludwig Schmidt, and Vaishaal Shankar. Do imagenet classifiers generalize to imagenet? In *International conference on machine learning*, pages 5389–5400. PMLR, 2019.
- Kuniaki Saito, Donghyun Kim, and Kate Saenko. Openmatch: Open-set semi-supervised learning with open-set consistency regularization. *Advances in Neural Information Processing Systems*, 34: 25956–25967, 2021.
- Shibani Santurkar, Dimitris Tsipras, and Aleksander Madry. Breeds: Benchmarks for subpopulation shift. 2020.
- Walter J Scheirer, Lalit P Jain, and Terrance E Boult. Probability models for open set recognition. *IEEE transactions on pattern analysis and machine intelligence*, 36(11):2317–2324, 2014.
- Alireza Shafaei, Mark Schmidt, and James J Little. A less biased evaluation of out-of-distribution sample detectors. *arXiv preprint arXiv:1809.04729*, 2018.
- Lavanya Sharan, Ruth Rosenholtz, and Edward H Adelson. Accuracy and speed of material categorization in real-world images. *Journal of vision*, 14(9):12–12, 2014.
- Mainak Singha, Harsh Pal, Ankit Jha, and Biplab Banerjee. Ad-clip: Adapting domains in prompt space using clip. In *Proceedings of the IEEE/CVF International Conference on Computer Vision*, pages 4355–4364, 2023.
- Lin Song, Ruoyi Xue, Hang Wang, Hongbin Sun, Yixiao Ge, Ying Shan, et al. Meta-adapter: An online few-shot learner for vision-language model. *Advances in Neural Information Processing Systems*, 36:55361–55374, 2023.
- Xin Sun, Zhenning Yang, Chi Zhang, Keck-Voon Ling, and Guohao Peng. Conditional gaussian distribution learning for open set recognition. In *Proceedings of the IEEE/CVF Conference on Computer Vision and Pattern Recognition*, pages 13480–13489, 2020.
- Yiyou Sun, Chuan Guo, and Yixuan Li. React: Out-of-distribution detection with rectified activations. *Advances in Neural Information Processing Systems*, 34:144–157, 2021.

- Yiyou Sun, Yifei Ming, Xiaojin Zhu, and Yixuan Li. Out-of-distribution detection with deep nearest neighbors. In *International Conference on Machine Learning*, pages 20827–20840. PMLR, 2022.
- Grant Van Horn, Oisin Mac Aodha, Yang Song, Yin Cui, Chen Sun, Alex Shepard, Hartwig Adam, Pietro Perona, and Serge Belongie. The inaturalist species classification and detection dataset. In *Proceedings of the IEEE conference on computer vision and pattern recognition*, pages 8769–8778, 2018.
- Haohan Wang, Songwei Ge, Zachary Lipton, and Eric P Xing. Learning robust global representations by penalizing local predictive power. *Advances in Neural Information Processing Systems*, 32, 2019.
- Haoqi Wang, Zhizhong Li, Litong Feng, and Wayne Zhang. Vim: Out-of-distribution with virtual-logit matching. In *Proceedings of the IEEE/CVF conference on computer vision and pattern recognition*, pages 4921–4930, 2022.
- Hualiang Wang, Yi Li, Huifeng Yao, and Xiaomeng Li. Clipn for zero-shot ood detection: Teaching clip to say no. In *Proceedings of the IEEE/CVF International Conference on Computer Vision*, pages 1802–1812, 2023a.
- Haoliang Wang, Chen Zhao, Yunhui Guo, Kai Jiang, and Feng Chen. Towards effective semantic ood detection in unseen domains: A domain generalization perspective. *arXiv preprint arXiv:2309.10209*, 2023b.
- Zhengbo Wang, Jian Liang, Ran He, Nan Xu, Zilei Wang, and Tieniu Tan. Improving zero-shot generalization for clip with synthesized prompts. In *Proceedings of the IEEE/CVF International Conference on Computer Vision*, pages 3032–3042, 2023c.
- Syed Talal Wasim, Muzammal Naseer, Salman Khan, Fahad Shahbaz Khan, and Mubarak Shah. Vita-clip: Video and text adaptive clip via multimodal prompting. In *Proceedings of the IEEE/CVF Conference on Computer Vision and Pattern Recognition*, pages 23034–23044, 2023.
- Mitchell Wortsman, Gabriel Ilharco, Samir Ya Gadre, Rebecca Roelofs, Raphael Gontijo-Lopes, Ari S Morcos, Hongseok Namkoong, Ali Farhadi, Yair Carmon, Simon Kornblith, et al. Model soups: averaging weights of multiple fine-tuned models improves accuracy without increasing inference time. In *International Conference on Machine Learning*, pages 23965–23998. PMLR, 2022.
- Jianxiong Xiao, James Hays, Krista A Ehinger, Aude Oliva, and Antonio Torralba. Sun database: Large-scale scene recognition from abbey to zoo. In *2010 IEEE computer society conference on computer vision and pattern recognition*, pages 3485–3492. IEEE, 2010.
- Zehao Xiao, Jiayi Shen, Mohammad Mahdi Derakhshani, Shengcai Liao, and Cees G. M. Snoek. Any-shift prompting for generalization over distributions. 2024.
- Jingkang Yang, Pengyun Wang, Dejian Zou, Zitang Zhou, Kunyuan Ding, Wenxuan Peng, Haoqi Wang, Guangyao Chen, Bo Li, Yiyou Sun, Xuefeng Du, Kaiyang Zhou, Wayne Zhang, Dan Hendrycks, Yixuan Li, and Ziwei Liu. Openood: Benchmarking generalized out-of-distribution detection. 2022.
- Jingkang Yang, Kaiyang Zhou, and Ziwei Liu. Full-spectrum out-of-distribution detection. *International Journal of Computer Vision*, 131(10):2607–2622, 2023.
- Nanyang Ye, Kaican Li, Lanqing Hong, Haoyue Bai, Yiting Chen, Fengwei Zhou, and Zhenguo Li. Ood-bench: Benchmarking and understanding out-of-distribution generalization datasets and algorithms. *CoRR*, abs/2106.03721, 2021.
- Hongjie Zhang, Ang Li, Jie Guo, and Yanwen Guo. Hybrid models for open set recognition. In *Computer Vision–ECCV 2020: 16th European Conference, Glasgow, UK, August 23–28, 2020, Proceedings, Part III 16*, pages 102–117. Springer, 2020.
- Jingyang Zhang, Jingkang Yang, Pengyun Wang, Haoqi Wang, Yueqian Lin, Haoran Zhang, Yiyou Sun, Xuefeng Du, Yixuan Li, Ziwei Liu, Yiran Chen, and Hai Li. Openood v1.5: Enhanced benchmark for out-of-distribution detection. *arXiv preprint arXiv:2306.09301*, 2023a.

- Renrui Zhang, Rongyao Fang, Peng Gao, Wei Zhang, Kunchang Li, Jifeng Dai, Yu Qiao, and Hongsheng Li. Tip-adapter: Training-free clip-adapter for better vision-language modeling. *arXiv preprint arXiv:2111.03930*, 2021a.
- Xin Zhang, Yusuke Iwasawa, Yutaka Matsuo, and Shixiang Shane Gu. Amortized prompt: Guide clip to domain transfer learning. *arXiv preprint arXiv:2111.12853*, 2021b.
- Yabin Zhang and Lei Zhang. Adaneg: Adaptive negative proxy guided ood detection with vision-language models. *arXiv preprint arXiv:2410.20149*, 2024.
- Yi Zhang, Ce Zhang, Xuetong Hu, and Zhihai He. Unsupervised prototype adapter for vision-language models. In *Chinese Conference on Pattern Recognition and Computer Vision (PRCV)*, pages 197–209. Springer, 2023b.
- Yabin Zhang, Wenjie Zhu, Chenhang He, and Lei Zhang. Lapt: Label-driven automated prompt tuning for ood detection with vision-language models. In *European Conference on Computer Vision*, pages 271–288. Springer, 2024.
- Bolei Zhou, Agata Lapedriza, Aditya Khosla, Aude Oliva, and Antonio Torralba. Places: A 10 million image database for scene recognition. *IEEE transactions on pattern analysis and machine intelligence*, 40(6):1452–1464, 2017.
- Kaiyang Zhou, Jingkang Yang, Chen Change Loy, and Ziwei Liu. Learning to prompt for vision-language models. *arXiv preprint arXiv:2109.01134*, 2021.
- Kaiyang Zhou, Jingkang Yang, Chen Change Loy, and Ziwei Liu. Conditional prompt learning for vision-language models. In *IEEE/CVF Conference on Computer Vision and Pattern Recognition (CVPR)*, 2022.
- Zhi Zhou, Ming Yang, Jiang-Xin Shi, Lan-Zhe Guo, and Yu-Feng Li. Decoop: Robust prompt tuning with out-of-distribution detection. *arXiv preprint arXiv:2406.00345*, 2024.
- Deyao Zhu, Jun Chen, Xiaoqian Shen, Xiang Li, and Mohamed Elhoseiny. Minigpt-4: Enhancing vision-language understanding with advanced large language models, 2023a.
- Lin Zhu, Xinbing Wang, Chenghu Zhou, and Nanyang Ye. Bayesian cross-modal alignment learning for few-shot out-of-distribution generalization. In *Proceedings of the AAAI Conference on Artificial Intelligence*, pages 11461–11469, 2023b.
- Lin Zhu, Yifeng Yang, Qinying Gu, Xinbing Wang, Chenghu Zhou, and Nanyang Ye. Croft: Robust fine-tuning with concurrent optimization for ood generalization and open-set ood detection. *arXiv preprint arXiv:2405.16417*, 2024.
- Lin Zhu, Yifeng Yang, Zichao Nie, Yuan Gao, Jiarui Li, Qinying Gu, Xinbing Wang, Chenghu Zhou, and Nanyang Ye. Infobound: A provable information-bounds inspired framework for both ood generalization and ood detection. *IEEE Transactions on Pattern Analysis and Machine Intelligence*, 2025a.
- Lin Zhu, Weihan Yin, Fan Wu, Qinying Gu, Xinbing Wang, Chenghu Zhou, and Nanyang Ye. Bayes-cal: Robust cross-modal alignment by bayesian approach for few-shot ood generalization. *International Journal of Computer Vision*, pages 1–34, 2025b.
- Yao Zhu, YueFeng Chen, Chuanlong Xie, Xiaodan Li, Rong Zhang, Hui Xue, Xiang Tian, Yaowu Chen, et al. Boosting out-of-distribution detection with typical features. *Advances in Neural Information Processing Systems*, 35:20758–20769, 2022.
- Bo Zong, Qi Song, Martin Renqiang Min, Wei Cheng, Cristian Lumezanu, Daeki Cho, and Haifeng Chen. Deep autoencoding gaussian mixture model for unsupervised anomaly detection. In *International conference on learning representations*, 2018.

A Related Works

Robust fine-tuning methods for VLM For training efficiency, there have been many lightweight CLIP-based fine-tuning methods to enhance generalization performance via prompt tuning (Singha et al., 2023; Huang et al., 2022; Khattak et al., 2023a; Wang et al., 2023c; Wasim et al., 2023; Goswami et al., 2024; Huang et al., 2024) or adapter tuning (Gondal et al., 2024; Zhang et al., 2023b; Song et al., 2023). Prompt tuning methods aim to get better vision-language alignment via only fine-tuning the input prompts. For example, with only few-shot samples for learning, CoOp (Zhou et al., 2021) improved significantly in generalization ability over intensively-tuned manual prompts via prompt learning. Motivated by learning generalization prompts, CoCoOp (Zhou et al., 2022) is proposed to achieve generalization on unseen classes via conditional prompt learning. Adapter-tuning is another popular lightweight fine-tuning method, like CLIP-Adapter (Gao et al., 2023), Tip-Adapter (Zhang et al., 2021a). Both of them inject a lightweight bottleneck architecture after the image encoder or text encoder and perform residual-style feature blending with the original pre-trained embeddings. However, most previous studies have focused on improving models’ robustness to covariate shifts, without being able to effectively address OOD detection.

Note that several studies, such as CoCoOp (Zhou et al., 2022), PromptSRC (Khattak et al., 2023b), SHIP (Wang et al., 2023c), and Promptkd (Li et al., 2024b), have explored the base-to-new ability of VLMs, aiming to improve VLMs’ classification performance to unseen classes. However, we emphasize that our approach differs from these methods in its handling of classes that were unseen during training. While these methods focus on classifying unseen classes, our method is designed specifically to detect these unseen classes without performing classification, ensuring safety in real-world applications. Although there have been several studies (Bai et al., 2023; Zhu et al., 2024) to handle OOD generalization and OOD detection simultaneously, these approaches are typically limited to traditional vision models or have been evaluated with a narrow set of post-hoc functions for OOD Detection. Thus, when fine-tuning VLMs for downstream tasks, the challenge of improving the models’ generalization ability to closed-set OOD data while simultaneously detecting open-set OOD classes that were unseen during fine-tuning remains largely underexplored.

OOD detection methods There are multiple lines of work addressing OOD detection, such as anomaly detection (Zong et al., 2018; Liang et al., 2017b), outlier detection (Bevandić et al., 2021; Saito et al., 2021), and open-set OOD recognition (Kong and Ramanan, 2021; Geng et al., 2020; Scheirer et al., 2014). These methods can be categorized into two main groups: post hoc methods (Zhu et al., 2022; Liu et al., 2020; Sun et al., 2021; Hendrycks and Gimpel, 2016; Liang et al., 2017b; Wang et al., 2022; Sun et al., 2022) and training-time regularization (Narayanaswamy et al., 2023; Bai et al., 2023; Malinin and Gales, 2018; Du et al., 2022b,a; Ming et al., 2022b). The former typically resort to post-hoc functions to recognize open-set without altering the DNN training process, like density estimation (Zhang et al., 2020), uncertainty modeling (Gal and Ghahramani, 2016), and input image reconstruction (Pidhorskyi et al., 2018; Sun et al., 2020). On the other hand, regularization-based methods aim to rectify the training process, compelling models to provide predictions with lower confidence. Recent studies (Zhou et al., 2024; Bai et al., 2024; Nie et al., 2024; Li et al., 2024a; Wang et al., 2023a; Miyai et al., 2024b; Zhang et al., 2024; Jiang et al., 2024; Ming et al., 2022a; Zhang and Zhang, 2024; Ming and Li, 2024) have explored the capability of zero-shot or few-shot OOD detection based on VLMs. More details about the CLIP-based OOD detection methods can be seen in these surveys (Miyai et al., 2024a; Li et al., 2025). However, while these studies primarily focus on handling semantic-shifted datasets, our research aims to simultaneously improve both OOD detection for semantic shifts and OOD generalization for covariate shifts, enabling more effective handling of diverse OOD datasets in real-world scenarios.

Full-spectrum OOD detection Recent works, such as OpenOOD v1.5 (Yang et al., 2022; Zhang et al., 2023a) and SEM (Yang et al., 2023), have taken into account both covariate shifts and semantic shifts and introduced full-spectrum OOD (FS-OOD) detection, which considers both detecting semantic shifts and being tolerant to covariate shifts. OpenOOD v1.5 extends benchmark evaluations to large-scale datasets (e.g., ImageNet) and foundation models (e.g., CLIP and DINOv2), broadening its scope to study FS-OOD detection under both types of distribution shifts. While the FS-OOD benchmark assesses OOD detection performance across diverse distribution types, it does not primarily focus on improving VLMs’ classification accuracy (i.e., OOD generalization) under covariate shifts. Moreover, in practical applications, there is a strong motivation to create models that can not only detect semantically shifted OOD inputs but also generalize to covariate-shifted data. Within CLIP-based

methods, OOD detection and generalization are often discussed in separate contexts, resulting in a trade-off between detection and generalization performance (Miyai et al., 2024a). In this paper, we focus on improving VLMs' OOD generalization ability on covariate-shifted OOD data while simultaneously detecting semantic-shifted samples. To substantiate the effectiveness of the proposed method for both tasks, we conduct an empirical analysis of distinct categories of competitive methods, including the CLIP-based zero-shot OOD detection method, lightweight tuning-based OOD detection methods, and lightweight tuning-based OOD generalization methods.

B Proof of Theorem 3.2

We first provide the proof for property (1) in Theorem 3.2. In this paper, we achieve re-aligning vision-language modalities by disrupting the top- c maximum cosine similarity to a low value. Let $\hat{y}_1 := \operatorname{argmax}_{i \in [K]} s_i(\mathbf{x}')$ denote the index of the maximum cosine similarity for an OOD input \mathbf{x}' . We then reduce the maximum cosine similarity to zero according to Equation 1 and denote the difference between the original and re-aligned cosine similarity as $\tilde{s}_{\hat{y}_1}(\mathbf{x}_i) - s_{\hat{y}_1}(\mathbf{x}_i) = \mu(\mathbf{x}_i)$.

Without loss of generality, we set $c = 1$, the energy score before re-alignment is denoted as $E_0(\mathbf{x}')$, which is calculated as:

$$E_0(\mathbf{x}') = -\log \sum_{i=1}^K e^{s_i(\mathbf{x}')/\tau} \quad (9)$$

The energy score after re-alignment is denoted as $E_1(\mathbf{x}')$, which is calculated as:

$$E_1(\mathbf{x}') = -\log \left[\sum_{i \neq \hat{y}_1} e^{s_i(\mathbf{x}')/\tau} + e^{\tilde{s}_{\hat{y}_1}(\mathbf{x}')/\tau} \right] \quad (10)$$

Given the ID class labels \mathcal{Y}_{in} , the newly proposed OOD score (ΔEnergy) is defined as:

$$\begin{aligned} S_{\Delta\text{Energy}}(\mathbf{x}'; \mathcal{Y}_{\text{in}}) &= E_1(\mathbf{x}') - E_0(\mathbf{x}') \\ &= -\log \left[\sum_{i \neq \hat{y}_1} e^{s_i(\mathbf{x}')/\tau} + e^{\tilde{s}_{\hat{y}_1}(\mathbf{x}')/\tau} \right] + \log \sum_{i=1}^K e^{s_i(\mathbf{x}')/\tau} \\ &= \log \frac{\sum_{i \neq \hat{y}_1} e^{s_i(\mathbf{x}')/\tau} + e^{\tilde{s}_{\hat{y}_1}(\mathbf{x}')/\tau} + e^{s_{\hat{y}_1}(\mathbf{x}')/\tau} - e^{\tilde{s}_{\hat{y}_1}(\mathbf{x}')/\tau}}{\sum_{i \neq \hat{y}_1} e^{s_i(\mathbf{x}')/\tau} + e^{\tilde{s}_{\hat{y}_1}(\mathbf{x}')/\tau}} \\ &= \log \left[1 + \frac{e^{s_{\hat{y}_1}(\mathbf{x}')/\tau} - e^{\tilde{s}_{\hat{y}_1}(\mathbf{x}')/\tau}}{\sum_{i \neq \hat{y}_1} e^{s_i(\mathbf{x}')/\tau} + e^{\tilde{s}_{\hat{y}_1}(\mathbf{x}')/\tau}} \right] \\ &= \log \left[1 + \frac{e^{s_{\hat{y}_1}(\mathbf{x}')/\tau} - e^{(s_{\hat{y}_1}(\mathbf{x}') - \mu(\mathbf{x}_i))/\tau}}{\sum_{i \neq \hat{y}_1} e^{s_i(\mathbf{x}')/\tau} + e^{(s_{\hat{y}_1}(\mathbf{x}') - \mu(\mathbf{x}_i))/\tau}} \right] \\ &= \log \left[1 + \frac{e^{\mu(\mathbf{x}_i)/\tau} - 1}{\frac{\sum_{i \neq \hat{y}_1} e^{s_i(\mathbf{x}')/\tau}}{e^{(s_{\hat{y}_1}(\mathbf{x}') - \mu(\mathbf{x}_i))/\tau}} + 1} \right] \end{aligned} \quad (11)$$

If we set $\tilde{s}_{\hat{y}_1}(\mathbf{x}') = 0$, i.e., $\mu(\mathbf{x}_i) = s_{\hat{y}_1}(\mathbf{x}')$, we have:

$$S_{\Delta\text{Energy}}(\mathbf{x}'; \mathcal{Y}_{\text{in}}) = E_1(\mathbf{x}') - E_0(\mathbf{x}') = \log \left[1 + \frac{e^{s_{\hat{y}_1}(\mathbf{x}')/\tau} - 1}{\sum_{i \neq \hat{y}_1} e^{s_i(\mathbf{x}')/\tau} + 1} \right] \quad (12)$$

Given the ID sample \mathbf{x}_{ID} and OOD sample \mathbf{x}_{OOD} , we assume that the sum of non-maximal cosine similarities is similar for ID and OOD samples, i.e., $\sum_{i \neq \hat{y}_1} e^{s_i(\mathbf{x}_{\text{ID}})/\tau} \approx \sum_{i \neq \hat{y}_1} e^{s_i(\mathbf{x}_{\text{OOD}})/\tau}$, which is reasonable under uniform similarity distributions as discussed in prior work (Ming et al., 2022a). Since the $S_{\Delta\text{Energy}}(\mathbf{x}; \mathcal{Y}_{\text{in}})$ is a monotonically increasing function with respect to the maximum similarity $s_{\hat{y}_1}(\mathbf{x})$, the energy change for ID data is greater than that for OOD data.

We then provide the more detailed results and proof for property (2) in Theorem 3.2 as follows:

Theorem B.1. [Difference Amplification between ID and OOD by Δ Energy] Let $S_{\Delta\text{Energy}}(\mathbf{x}, \mathcal{Y}_{\text{in}})$ and $S_{\Delta\text{MCM}}(\mathbf{x}, \mathcal{Y}_{\text{in}})$ be the OOD score for any sample \mathbf{x} by the Δ Energy and MCM method, respectively, where:

$$S_{\Delta\text{Energy}}(\mathbf{x}; \mathcal{Y}_{\text{in}}) = E_1(\mathbf{x}) - E_0(\mathbf{x}) = \log \left[1 + \frac{e^{s_{\hat{y}_1}(\mathbf{x})/\tau} - 1}{\sum_{i \neq \hat{y}_1} e^{s_i(\mathbf{x})/\tau} + 1} \right] \quad (13)$$

$$S_{\Delta\text{MCM}}(\mathbf{x}; \mathcal{Y}_{\text{in}}) = \frac{e^{s_{\hat{y}_1}(\mathbf{x})/\tau}}{e^{s_{\hat{y}_1}(\mathbf{x})/\tau} + \sum_{i \neq \hat{y}_1} e^{s_i(\mathbf{x})/\tau}} \quad (14)$$

Suppose that the maximum cosine similarity for an ID sample \mathbf{x}_{ID} is greater than that of an OOD sample \mathbf{x}_{OOD} , i.e., $s_{\hat{y}_1}(\mathbf{x}_{\text{ID}}) > s_{\hat{y}_1}(\mathbf{x}_{\text{OOD}})$. We also assume that the sum of non-maximal cosine similarities is similar for ID and OOD samples, i.e., $\sum_{i \neq \hat{y}_1} e^{s_i(\mathbf{x}_{\text{ID}})/\tau} \approx \sum_{i \neq \hat{y}_1} e^{s_i(\mathbf{x}_{\text{OOD}})/\tau}$, which is reasonable under uniform similarity distributions as discussed in prior work (Ming et al., 2022a). Then the difference between ID and OOD under Δ Energy exceeds that of the MCM method:

$$d_{\Delta\text{Energy}} > d_{\text{MCM}}$$

where $d_{\Delta\text{Energy}} = S_{\Delta\text{Energy}}(\mathbf{x}_{\text{ID}}; \mathcal{Y}_{\text{in}}) - S_{\Delta\text{Energy}}(\mathbf{x}_{\text{OOD}}; \mathcal{Y}_{\text{in}})$, and $d_{\text{MCM}} = S_{\Delta\text{MCM}}(\mathbf{x}_{\text{ID}}; \mathcal{Y}_{\text{in}}) - S_{\Delta\text{MCM}}(\mathbf{x}_{\text{OOD}}; \mathcal{Y}_{\text{in}})$. Thus, our Δ Energy exhibits strictly stronger separability between ID and OOD distributions.

Proof: Let $s = s_i(\mathbf{x})/\tau$, we simplify the Δ Energy score as $S_{\Delta\text{Energy}}(\mathbf{x}, \mathcal{Y}_{\text{in}}) = \log(1 + \frac{e^s - 1}{b+1})$ and simplify the MCM score as $S_{\Delta\text{MCM}}(\mathbf{x}; \mathcal{Y}_{\text{in}}) = \frac{e^s}{e^s + b}$ where $b = \sum_{i \neq \hat{y}_1} e^{s_i(\mathbf{x})/\tau}$.

First, we analyze the gradient with respect to $s_{\hat{y}_1}$:

$$\frac{\partial S_{\Delta\text{Energy}}}{\partial s_{\hat{y}_1}} = \frac{1}{\tau} \cdot \frac{e^{s_{\hat{y}_1}/\tau}}{e^{s_{\hat{y}_1}/\tau} + b} = \frac{1}{\tau} S_{\text{MCM}} \quad (15)$$

$$\frac{\partial S_{\text{MCM}}}{\partial s_{\hat{y}_1}} = \frac{1}{\tau} \cdot \frac{e^{s_{\hat{y}_1}/\tau} b}{(e^{s_{\hat{y}_1}/\tau} + b)^2} = \frac{1}{\tau} S_{\text{MCM}}(1 - S_{\text{MCM}}) \quad (16)$$

Since $0 < S_{\text{MCM}} \leq 1$, we have $\frac{\partial S_{\Delta\text{Energy}}}{\partial s_{\hat{y}_1}} > \frac{\partial S_{\text{MCM}}}{\partial s_{\hat{y}_1}}$ and $d_{\Delta\text{Energy}} > d_{\text{MCM}}$.

Next, we consider the large-scale setting where the number of ID classes K is large. Let $b \approx \sum_{i \neq \hat{y}_1} e^{s_i(\mathbf{x})/\tau}$. In this case, the denominator term b becomes significantly larger than the maximum similarity term, i.e., $b \gg e^s$. We then perform Taylor Expansion for $S_{\Delta\text{Energy}}(\mathbf{x}, \mathcal{Y}_{\text{in}})$ and $S_{\Delta\text{MCM}}(\mathbf{x}, \mathcal{Y}_{\text{in}})$.

Taylor Expansion of $S_{\Delta\text{Energy}}(\mathbf{x}, \mathcal{Y}_{\text{in}})$: For $b \gg e^s$, we approximate $S_{\Delta\text{Energy}}(\mathbf{x}, \mathcal{Y}_{\text{in}})$ using $\log(1 + \epsilon) \approx \epsilon - \frac{\epsilon^2}{2}$: $S_{\Delta\text{Energy}}(\mathbf{x}, \mathcal{Y}_{\text{in}}) \approx \frac{e^s}{b} - \frac{e^{2s}}{2b^2}$.

Taylor Expansion of $S_{\Delta\text{MCM}}(\mathbf{x}, \mathcal{Y}_{\text{in}})$: Similarly, we expand $S_{\Delta\text{MCM}}(\mathbf{x}, \mathcal{Y}_{\text{in}})$: $S_{\Delta\text{MCM}}(\mathbf{x}, \mathcal{Y}_{\text{in}}) = \frac{e^s}{e^s + b} \approx \frac{e^s}{b} - \frac{e^{2s}}{b^2}$.

Then we can compute the difference between ID and OOD under the Δ Energy and MCM score, respectively:

$$d_{\Delta\text{Energy}} \approx \left(\frac{e^{s_{\hat{y}_1}(\mathbf{x}_{\text{ID}})/\tau}}{b} - \frac{e^{s_{\hat{y}_1}(\mathbf{x}_{\text{OOD}})/\tau}}{b} \right) - \frac{1}{2} \left(\frac{e^{2s_{\hat{y}_1}(\mathbf{x}_{\text{ID}})/\tau}}{b^2} - \frac{e^{2s_{\hat{y}_1}(\mathbf{x}_{\text{OOD}})/\tau}}{b^2} \right) \quad (17)$$

$$d_{\text{MCM}} \approx \left(\frac{e^{s_{\hat{y}_1}(\mathbf{x}_{\text{ID}})/\tau}}{b} - \frac{e^{s_{\hat{y}_1}(\mathbf{x}_{\text{OOD}})/\tau}}{b} \right) - \left(\frac{e^{2s_{\hat{y}_1}(\mathbf{x}_{\text{ID}})/\tau}}{b^2} - \frac{e^{2s_{\hat{y}_1}(\mathbf{x}_{\text{OOD}})/\tau}}{b^2} \right) \quad (18)$$

which leads to the following property:

$$d_{\Delta\text{Energy}} - d_{\text{MCM}} \approx \frac{e^{2s_{\hat{y}_1}(\mathbf{x}_{\text{ID}})/\tau} - e^{2s_{\hat{y}_1}(\mathbf{x}_{\text{OOD}})/\tau}}{2b^2} > 0 \quad (\text{since } s_{\hat{y}_1}(\mathbf{x}_{\text{ID}}) > s_{\hat{y}_1}(\mathbf{x}_{\text{OOD}})) \quad (19)$$

In large-scale hard OOD detection scenarios where $s_{\hat{y}_1}(\mathbf{x}_{\text{ID}}) - s_{\hat{y}_1}(\mathbf{x}_{\text{OOD}}) \ll 1$ (small maximum similarity gap) and $K \gg s_{\hat{y}_1}(\mathbf{x}_{\text{ID}}) > s_{\hat{y}_1}(\mathbf{x}_{\text{OOD}})$. As demonstrated in Equation 17 and Equation 18, ΔEnergy 's logarithmic form introduces a less aggressive decay in the higher-order term compared to MCM, preserving discriminability. For large K , MCM's separability diminishes quadratically ($\mathcal{O}(1/K^2)$), while ΔEnergy decays more slowly due to the smaller coefficient in the second-order term. Thus, ΔEnergy is better for large-scale OOD detection where K is large and the maximum similarity gap is small ($s_{\hat{y}_1}(\mathbf{x}_{\text{ID}}) - s_{\hat{y}_1}(\mathbf{x}_{\text{OOD}}) \ll 1$).

C Proof of Theorem 3.3

In Theorem 3.3, we provide formal guarantees that the proposed ΔEnergy can provably reduce the false positive rate (FPR) compared to the widely-used VLM-based OOD detection method MCM (Ming et al., 2022a). Before the proof of Theorem 3.3, we first introduce the MCM method as follows:

For any test input \mathbf{x}' , we calculate the label-wise matching score based on the cosine similarity between the image feature $\mathbf{z}_I(\mathbf{x}')$ and the concept vector (text feature) $\mathbf{z}_T(t_i)$: $s_i(\mathbf{x}') = \mathbf{z}_I(\mathbf{x}') \cdot \mathbf{z}_T(t_i)$. Note that both the image feature $\mathbf{z}_I(\mathbf{x}')$ and the concept vector $\mathbf{z}_T(t_i)$ are normalized features in this paper. The maximum concept matching (MCM) score is computed as follows:

$$S_{\text{MCM}}(\mathbf{x}'; \mathcal{Y}_{\text{in}}) = \max_i \frac{e^{s_i(\mathbf{x}')/\tau}}{\sum_{j=1}^K e^{s_j(\mathbf{x}')/\tau}},$$

Under the Assumption C.1, Ming et.al (Ming et al., 2022a) have provided the formal guarantees for MCM that using softmax can provably reduce the false positive rate (FPR) compared to that without softmax, as illustrated in Theorem C.2.

Assumption C.1. [(Ming et al., 2022a)] Let $z := 1\{y \in \mathcal{Y}_{\text{in}}\}$. $Q_{\mathbf{x}}$ denotes the out-of-distribution $\mathbb{P}_{\mathbf{x}|z=0}$ (marginal distribution of \mathbf{x} conditioned on $z = 0$). Assume $\exists \delta > 0$ such that

$$Q_{\mathbf{x}} \left(\frac{1}{K-1} \sum_{i \neq \hat{y}_1} [s_{\hat{y}_2}(\mathbf{x}) - s_i(\mathbf{x})] \leq \delta \right) = 1,$$

where $\hat{y}_1 := \text{argmax}_{i \in [K]} s_i(\mathbf{x})$ and $\hat{y}_2 := \text{argmax}_{i \neq \hat{y}_1, i \in [K]} s_i(\mathbf{x})$ denote the indices of the largest and second-largest cosine similarities for an OOD input \mathbf{x} .

Theorem C.2. [(Ming et al., 2022a)] Given a task with ID label set $\mathcal{Y}_{\text{in}} = \{y_1, y_2, \dots, y_K\}$ and a pre-trained VLM. If $Q_{\mathbf{x}}$ satisfies Assumption C.1, then there exists a constant $T = \frac{\lambda(K-1)(\lambda^{\text{wo}} + \delta - s_{\hat{y}_2})}{K\lambda - 1}$ such that for any temperature $\tau > T$, we have

$$\text{FPR}(\tau, \lambda) \leq \text{FPR}^{\text{wo}}(\lambda^{\text{wo}}),$$

where $\text{FPR}(\tau, \lambda)$ is the false positive rate based on softmax scaling with temperature τ and detection threshold λ ; $\text{FPR}^{\text{wo}}(\lambda^{\text{wo}})$ is the false positive rate without softmax scaling based on threshold λ^{wo} .

Now we present the proof of Theorem 3.3 as follows:

Proof: The newly proposed OOD score (ΔEnergy) is defined as:

$$\begin{aligned}
S_{\Delta\text{Energy}}(\mathbf{x}'; \mathcal{Y}_{\text{in}}) &= E_1 - E_0 \\
&= -\log \left[\sum_{i \neq \hat{y}_1} e^{s_i(\mathbf{x}')/\tau} + e^{\tilde{s}_{\hat{y}_1}(\mathbf{x}')/\tau} \right] + \log \sum_{i=1}^K e^{s_i(\mathbf{x}')/\tau} \\
&= \log \frac{\sum_{i \neq \hat{y}_1} e^{s_i(\mathbf{x}')/\tau} + e^{\tilde{s}_{\hat{y}_1}(\mathbf{x}')/\tau} + e^{s_{\hat{y}_1}(\mathbf{x}')/\tau} - e^{\tilde{s}_{\hat{y}_1}(\mathbf{x}')/\tau}}{\sum_{i \neq \hat{y}_1} e^{s_i(\mathbf{x}')/\tau} + e^{\tilde{s}_{\hat{y}_1}(\mathbf{x}')/\tau}} \\
&= \log \left[1 + \frac{e^{s_{\hat{y}_1}(\mathbf{x}')/\tau} - e^{\tilde{s}_{\hat{y}_1}(\mathbf{x}')/\tau}}{\sum_{i \neq \hat{y}_1} e^{s_i(\mathbf{x}')/\tau} + e^{\tilde{s}_{\hat{y}_1}(\mathbf{x}')/\tau}} \right] \\
&\leq \frac{e^{s_{\hat{y}_1}(\mathbf{x}')/\tau} - e^{\tilde{s}_{\hat{y}_1}(\mathbf{x}')/\tau}}{\sum_{i \neq \hat{y}_1} e^{s_i(\mathbf{x}')/\tau} + e^{\tilde{s}_{\hat{y}_1}(\mathbf{x}')/\tau}} = \frac{e^{s_{\hat{y}_1}(\mathbf{x}')/\tau} - e^{\tilde{s}_{\hat{y}_1}(\mathbf{x}')/\tau}}{\sum_{i=1}^K e^{s_i(\mathbf{x}')/\tau} + e^{\tilde{s}_{\hat{y}_1}(\mathbf{x}')/\tau} - e^{s_{\hat{y}_1}(\mathbf{x}')/\tau}} \\
&\leq \frac{e^{s_{\hat{y}_1}(\mathbf{x}')/\tau}}{\sum_{i=1}^K e^{s_i(\mathbf{x}')/\tau} + 2e^{\tilde{s}_{\hat{y}_1}(\mathbf{x}')/\tau} - e^{s_{\hat{y}_1}(\mathbf{x}')/\tau}}
\end{aligned} \tag{20}$$

When $c \in \{2, \dots, K\}$, without loss of generality, we take $c = 2$ as example and we have:

$$\begin{aligned}
S_{\Delta\text{Energy}}(\mathbf{x}'; \mathcal{Y}_{\text{in}}) &= E_1 - E_0 \\
&= \frac{1}{2} \left[-\log \left[\sum_{i \neq \hat{y}_1} e^{s_i(\mathbf{x}')/\tau} + e^{\tilde{s}_{\hat{y}_1}(\mathbf{x}')/\tau} \right] + \log \sum_{i=1}^K e^{s_i(\mathbf{x}')/\tau} \right] \\
&\quad + \frac{1}{2} \left[-\log \left[\sum_{i \neq \hat{y}_2} e^{s_i(\mathbf{x}')/\tau} + e^{\tilde{s}_{\hat{y}_2}(\mathbf{x}')/\tau} \right] + \log \sum_{i=1}^K e^{s_i(\mathbf{x}')/\tau} \right] \\
&\leq \frac{1}{2} \frac{e^{s_{\hat{y}_1}(\mathbf{x}')/\tau}}{\sum_{i=1}^K e^{s_i(\mathbf{x}')/\tau} + 2e^{\tilde{s}_{\hat{y}_1}(\mathbf{x}')/\tau} - e^{s_{\hat{y}_1}(\mathbf{x}')/\tau}} \\
&\quad + \frac{1}{2} \frac{e^{s_{\hat{y}_2}(\mathbf{x}')/\tau}}{\sum_{i=1}^K e^{s_i(\mathbf{x}')/\tau} + 2e^{\tilde{s}_{\hat{y}_2}(\mathbf{x}')/\tau} - e^{s_{\hat{y}_2}(\mathbf{x}')/\tau}}
\end{aligned} \tag{21}$$

For $c = 1$, if $2e^{\tilde{s}_{\hat{y}_1}(\mathbf{x}')/\tau} - e^{s_{\hat{y}_1}(\mathbf{x}')/\tau} \geq 0$, i.e., $s_{\hat{y}_1}(\mathbf{x}') - \tilde{s}_{\hat{y}_1}(\mathbf{x}') \leq \tau \ln 2$, we have

$$S_{\Delta\text{Energy}}(\mathbf{x}'; \mathcal{Y}_{\text{in}}) \leq \frac{e^{s_{\hat{y}_1}(\mathbf{x}')/\tau}}{\sum_{i=1}^K e^{s_i(\mathbf{x}')/\tau} + 2e^{\tilde{s}_{\hat{y}_1}(\mathbf{x}')/\tau} - e^{s_{\hat{y}_1}(\mathbf{x}')/\tau}} \leq \frac{e^{s_{\hat{y}_1}(\mathbf{x}')/\tau}}{\sum_{i=1}^K e^{s_i(\mathbf{x}')/\tau}} = S_{\text{MCM}}(\mathbf{x}'; \mathcal{Y}_{\text{in}})$$

For $c = 2$, we have $s_{\hat{y}_2}(\mathbf{x}') \leq s_{\hat{y}_1}(\mathbf{x}')$, if $2e^{\tilde{s}_{\hat{y}_2}(\mathbf{x}')/\tau} - e^{s_{\hat{y}_2}(\mathbf{x}')/\tau} \geq 0$, i.e., $s_{\hat{y}_2}(\mathbf{x}') - \tilde{s}_{\hat{y}_2}(\mathbf{x}') \leq \tau \ln 2$, we have

$$\begin{aligned}
\frac{e^{s_{\hat{y}_2}(\mathbf{x}')/\tau}}{\sum_{i=1}^K e^{s_i(\mathbf{x}')/\tau} + 2e^{\tilde{s}_{\hat{y}_2}(\mathbf{x}')/\tau} - e^{s_{\hat{y}_2}(\mathbf{x}')/\tau}} &\leq \frac{e^{s_{\hat{y}_1}(\mathbf{x}')/\tau}}{\sum_{i=1}^K e^{s_i(\mathbf{x}')/\tau} + 2e^{\tilde{s}_{\hat{y}_2}(\mathbf{x}')/\tau} - e^{s_{\hat{y}_2}(\mathbf{x}')/\tau}} \\
&\leq \frac{e^{s_{\hat{y}_1}(\mathbf{x}')/\tau}}{\sum_{i=1}^K e^{s_i(\mathbf{x}')/\tau}} = S_{\text{MCM}}(\mathbf{x}'; \mathcal{Y}_{\text{in}})
\end{aligned} \tag{22}$$

which leads to

$$S_{\Delta\text{Energy}}(\mathbf{x}'; \mathcal{Y}_{\text{in}}) \leq S_{\text{MCM}}(\mathbf{x}'; \mathcal{Y}_{\text{in}})$$

Let the OOD detection functions be represented by:

$$G(\mathbf{x}'; \mathcal{Y}_{\text{in}}) = \begin{cases} 1 & S_{\Delta\text{Energy}}(\mathbf{x}'; \mathcal{Y}_{\text{in}}) \geq \lambda \\ 0 & S_{\Delta\text{Energy}}(\mathbf{x}'; \mathcal{Y}_{\text{in}}) < \lambda \end{cases}, \tag{23}$$

then we have

$$\begin{aligned}
\text{FPR}^{\Delta\text{Energy}}(\tau, \lambda) &= \mathbb{P}(G(\mathbf{x}'; \mathcal{Y}_{\text{in}}) = 1 \mid z = 0) \\
&= Q_{\mathbf{x}'}(G(\mathbf{x}'; \mathcal{Y}_{\text{in}}) = 1) \\
&= Q_{\mathbf{x}'}(S_{\Delta\text{Energy}}(\mathbf{x}'; \mathcal{Y}_{\text{in}}) > \lambda) \\
&\leq Q_{\mathbf{x}'}(S_{\text{MCM}}(\mathbf{x}'; \mathcal{Y}_{\text{in}}) > \lambda) = \text{FPR}^{\text{MCM}}(\tau, \lambda)
\end{aligned} \tag{24}$$

Thus, we complete the proof.

D Proof of Theorem 3.4

Proof: To further enlarge the energy change between the masked VLM and unmasked VLM for closed-set classes, we propose to minimize the following loss:

$$\mathcal{L}_{\Delta E} = \frac{1}{N} \sum_{i=1}^N E_2(\mathbf{x}_i) - E_0(\mathbf{x}_i) \tag{25}$$

where $E_2(\mathbf{x}_i)$ is the energy score for \mathbf{x}_i after masking on the image feature, which is formally calculated as:

$$\begin{aligned}
E_2(\mathbf{x}_i) &= -\log \sum_{j=1}^K e^{s'_j(\mathbf{x}_i)} \\
s'_j(\mathbf{x}_i) &= (\mathbf{z}_I(\mathbf{x}_i) \odot \mathbf{m}'(\mathbf{x}_i)) \cdot \mathbf{z}_T(t_j)
\end{aligned}$$

where $\mathbf{m}'(\mathbf{x}_i)$ is the mask that retains the top p -proportion elements in $\mathbf{z}_I(\mathbf{x}_i) \odot \mathbf{h}_1(\mathbf{x}_i)$

Now we prove that $-\mathcal{L}_{\Delta E}$ is the lower bound of $\sum_{i=1}^N \Delta\text{Energy}(\mathbf{x}_i)$. Here, we represent the optimization term for \mathbf{x}_i as: $\mathcal{L}_{\Delta E}(\mathbf{x}_i) := E_2(\mathbf{x}_i) - E_0(\mathbf{x}_i)$. Then the relationship between $\Delta\text{Energy}(\mathbf{x}_i)$ and $\mathcal{L}_{\Delta E}(\mathbf{x}_i)$ can be formulated as:

$$\begin{aligned}
e^{\Delta\text{Energy}(\mathbf{x}_i)} - e^{-\mathcal{L}_{\Delta E}(\mathbf{x}_i)} &= \frac{\sum_{j=1}^K e^{s_j(\mathbf{x}_i)/\tau}}{\sum_{j \neq \hat{y}_1} e^{s_j(\mathbf{x}_i)/\tau} + e^{\tilde{s}_{\hat{y}_1}(\mathbf{x}_i)/\tau}} - \frac{\sum_{j \neq \hat{y}_1} e^{s'_j(\mathbf{x}_i)/\tau} + e^{s'_{\hat{y}_1}(\mathbf{x}_i)/\tau}}{\sum_{j=1}^K e^{s_j(\mathbf{x}_i)/\tau}} \\
&= \frac{\sum_{j=1}^K e^{s_j(\mathbf{x}_i)/\tau}}{\sum_{j \neq \hat{y}_1} e^{s_j(\mathbf{x}_i)/\tau} + e^{\tilde{s}_{\hat{y}_1}(\mathbf{x}_i)/\tau}} - \frac{\sum_{j \neq \hat{y}_1} e^{s'_j(\mathbf{x}_i)/\tau} + e^{s'_{\hat{y}_1}(\mathbf{x}_i)/\tau}}{\sum_{j=1}^K e^{s_j(\mathbf{x}_i)/\tau}} \\
&= \frac{e^{s_{\hat{y}_1}(\mathbf{x}_i)/\tau} - e^{\tilde{s}_{\hat{y}_1}(\mathbf{x}_i)/\tau}}{\sum_{j \neq \hat{y}_1} e^{s_j(\mathbf{x}_i)/\tau} + e^{\tilde{s}_{\hat{y}_1}(\mathbf{x}_i)/\tau}} - \frac{\sum_{j=1}^K [e^{s'_j(\mathbf{x}_i)/\tau} - e^{s_j(\mathbf{x}_i)/\tau}]}{\sum_{j=1}^K e^{s_j(\mathbf{x}_i)/\tau}} \\
&\geq \frac{e^{s_{\hat{y}_1}(\mathbf{x}_i)/\tau} - e^{\tilde{s}_{\hat{y}_1}(\mathbf{x}_i)/\tau}}{\sum_{j \neq \hat{y}_1} e^{s_j(\mathbf{x}_i)/\tau} + e^{\tilde{s}_{\hat{y}_1}(\mathbf{x}_i)/\tau}} - \frac{\sum_{j=1}^K [e^{s'_j(\mathbf{x}_i)/\tau} - e^{s_j(\mathbf{x}_i)/\tau}]}{\sum_{j=1}^K e^{s_j(\mathbf{x}_i)/\tau}}
\end{aligned} \tag{26}$$

where the inequality in the last line follows $\tilde{s}_{\hat{y}_1}(\mathbf{x}_i) \leq s_{\hat{y}_1}(\mathbf{x}_i)$.

Under the condition that $e^{s_{\hat{y}_1}(\mathbf{x}_i)/\tau} - e^{\tilde{s}_{\hat{y}_1}(\mathbf{x}_i)/\tau} \geq (e^{\varepsilon_E} - 1) \sum_{j=1}^K e^{s'_j(\mathbf{x}_i)/\tau} = (e^{\varepsilon_E} - 1) e^{-E_2(\mathbf{x}_i)}$ and that $\mathcal{L}_{\Delta E} \leq \varepsilon_E$, it is straightforward to derive the following inequality:

$$e^{s_{\hat{y}_1}(\mathbf{x}_i)/\tau} - e^{\tilde{s}_{\hat{y}_1}(\mathbf{x}_i)/\tau} \geq \sum_{j=1}^K [e^{s'_j(\mathbf{x}_i)/\tau} - e^{s_j(\mathbf{x}_i)/\tau}]$$

Thus we have $\Delta\text{Energy}(\mathbf{x}_i) \geq -\mathcal{L}_{\Delta E}(\mathbf{x}_i)$. Thus complete the proof.

E Proof of Theorem 3.5

Proof: In the prompt-tuning framework of our proposed EBM, only n context vectors are learnable, and we denote the learnable context vectors as $\theta = [\theta_1, \dots, \theta_n]$. The $\mathcal{L}_{\Delta E}$ can be represented by:

$$\mathcal{L}_{\Delta E} = \frac{1}{N} \sum_{i=1}^N \left(\log \sum_{j=1}^K \exp \langle \mathbf{z}_I(\mathbf{x}_i), \mathbf{z}_T(t_j; \theta) \rangle - \log \sum_{j=1}^K \exp \langle \mathbf{m}_I(\mathbf{x}_i), \mathbf{z}_T(t_j; \theta) \rangle \right) \tag{27}$$

where $\mathbf{m}_I(\mathbf{x}_i) = \mathbf{z}_I(\mathbf{x}_i) \odot \mathbf{m}'(\mathbf{x}_i)$ is the masked image feature. Now we expand $\nabla_\theta \mathcal{L}_{\Delta E}$ as follows:

$$\nabla_\theta \mathcal{L}_{\Delta E} = \frac{1}{N} \sum_{i=1}^N \left[\frac{\nabla_\theta \sum_{j=1}^K \exp \langle \mathbf{z}_I(\mathbf{x}_i), \mathbf{z}_T(t_j; \theta) \rangle}{\sum_{j=1}^K \exp \langle \mathbf{z}_I(\mathbf{x}_i), \mathbf{z}_T(t_j; \theta) \rangle} - \frac{\nabla_\theta \sum_{j=1}^K \exp \langle \mathbf{m}_I(\mathbf{x}_i), \mathbf{z}_T(t_j; \theta) \rangle}{\sum_{j=1}^K \exp \langle \mathbf{m}_I(\mathbf{x}_i), \mathbf{z}_T(t_j; \theta) \rangle} \right] \quad (28)$$

We denote

$$\mathbf{a}_0 = \frac{1}{N} \sum_{i=1}^N \left(\log \sum_{j=1}^K \exp \langle \mathbf{z}_I(\mathbf{x}_i), \mathbf{z}_T(t_j; \theta) \rangle \right)$$

$$\mathbf{a}_1 = \frac{1}{N} \sum_{i=1}^N \left(\log \sum_{j=1}^K \exp \langle \mathbf{m}_I(\mathbf{x}_i), \mathbf{z}_T(t_j; \theta) \rangle \right)$$

Then we have $\nabla_\theta \mathcal{L}_{\Delta E} = \nabla_\theta \mathbf{a}_0 - \nabla_\theta \mathbf{a}_1$. The local optimization of $\mathcal{L}_{\Delta E}$ lead to $\nabla_\theta \mathbf{a}_0 = \nabla_\theta \mathbf{a}_1$.

Let $S^{(i)}$ represent the cosine similarity between the image feature $\mathbf{z}_I(\mathbf{x}_i)$ and the text feature corresponding to its ground-truth label. The empirical classification loss, $\mathcal{E}_D(\theta)$, can be calculated as:

$$\begin{aligned} \mathcal{E}_D(\theta) &= -\frac{1}{N} \sum_{i=1}^N \log \frac{\exp S^{(i)}}{\sum_{j=1}^K \exp \langle \mathbf{z}_I(\mathbf{x}_i), \mathbf{z}_T(t_j; \theta) \rangle} \\ &= \frac{1}{N} \sum_{i=1}^N \left[\log \sum_{j=1}^K \exp \langle \mathbf{z}_I(\mathbf{x}_i), \mathbf{z}_T(t_j; \theta) \rangle - S^{(i)} \right] \end{aligned} \quad (29)$$

Accordingly, the gradient vector of empirical risk $\widehat{\mathcal{E}}_D(\theta)$ with respect to parameter θ is represented as:

$$\widehat{\mathbf{G}}_D(\theta) = \nabla_\theta \widehat{\mathcal{E}}_D(\theta) = \frac{1}{N} \sum_{i=1}^N \left[\frac{\nabla_\theta \sum_{j=1}^K \exp \langle \mathbf{z}_I(\mathbf{x}_i), \mathbf{z}_T(t_j; \theta) \rangle}{\sum_{j=1}^K \exp \langle \mathbf{z}_I(\mathbf{x}_i), \mathbf{z}_T(t_j; \theta) \rangle} - \nabla_\theta S^{(i)} \right] = -\mathbf{a} - \frac{1}{N} \sum_{i=1}^N \nabla_\theta S^{(i)} \quad (30)$$

And the Hessian matrix of empirical risk with respect to parameter θ is calculated as:

$$\widehat{\mathbf{H}}_D(\theta) = \nabla_\theta^2 \widehat{\mathcal{E}}_D(\theta) = -\nabla_\theta \mathbf{a} - \frac{1}{N} \sum_{i=1}^N \nabla_\theta^2 S^{(i)} \quad (31)$$

The local optimum solution of Equation 4, i.e., $\nabla_\theta \mathcal{L}_{\Delta E} = \mathbf{0}$, gives the following equation:

$$\widehat{\mathbf{H}}_S(\theta) - \widehat{\mathbf{H}}_{S'}(\theta) = -\frac{1}{N} \sum_{i=1}^N (\nabla_\theta^2 S^{(i)} - \nabla_\theta^2 S_m^{(i)}) = -\frac{1}{N} \sum_{i=1}^N \nabla_\theta^2 [(\mathbf{z}_I(\mathbf{x}_i) - \mathbf{m}_I^{(i)}) \cdot \mathbf{z}_T(\mathbf{x}_i)] \quad (32)$$

Finally, we can conclude that the local optimum solution of Equation 4 leads to the following property:

$$|\theta^\top (\widehat{\mathbf{H}}_S(\theta) - \widehat{\mathbf{H}}_{S'}(\theta))\theta| = |\theta^\top \frac{1}{N} \sum_{i=1}^N \nabla_\theta^2 [(\mathbf{z}_I(\mathbf{x}_i) - \mathbf{m}_I^{(i)}) \cdot \mathbf{z}_T(\mathbf{x}_i)]\theta| \leq O(\varepsilon) \quad (33)$$

F Proof of Proposition 3.6

Proof: Let θ^* be the local minimum across all domains, i.e., $\nabla_\theta \widehat{\mathcal{E}}_D(\theta^*) = \mathbf{0}$, and $\mathcal{D} = \{\mathcal{S}, \mathcal{T}\}$. By Taylor expansion, the OOD generalization gap between source domain (\mathcal{S}) and target domain (\mathcal{T}) is

Table 5: **Conventional OOD detection Results:** OOD detection performance for ImageNet-1k as ID. In the table, we extend our Δ Energy method to the zero-shot method CSP, leveraging the informative information from extra OOD labels as detailed in Equation 36.

Method	Texture		iNaturalist		Places		SUN		Avg	
	AUC \uparrow	FPR95 \downarrow								
CLIP-based post-hoc methods										
MSP	74.84	73.66	77.74	74.57	72.18	79.12	73.97	76.95	74.98	76.22
MaxLogit	88.63	48.72	88.03	60.88	87.45	55.54	91.16	44.83	88.82	52.49
Energy	88.22	50.39	87.18	64.98	87.33	57.40	91.17	46.42	88.48	54.80
ReAct	88.13	49.88	86.87	65.57	87.42	56.85	91.04	46.17	88.37	54.62
ODIN	87.85	51.67	94.65	30.22	85.54	55.06	87.17	54.04	88.80	47.75
Tuning-based methods										
NegPrompt	91.60	35.21	98.73	6.32	93.34	27.60	95.55	22.89	94.81	23.01
ID-Like	94.32	25.27	98.19	8.98	91.15	41.74	91.64	42.03	93.83	29.51
LoCoOp	90.19	42.28	96.86	16.05	91.98	32.87	95.07	23.44	93.52	28.66
LSN+CoOp	89.52	31.57	95.47	23.48	90.87	36.43	93.45	29.84	92.33	31.97
LSN+CoCoOp	90.42	38.54	95.83	21.56	91.25	34.48	94.35	26.32	92.96	30.22
GallLoP	90.40	38.40	97.10	13.70	91.30	32.50	94.00	24.90	93.20	27.30
Zero-shot methods										
MCM	86.11	57.77	94.61	30.91	89.77	44.69	92.57	34.59	90.76	42.74
CLIPN	90.93	40.83	95.27	23.94	92.28	33.45	93.92	26.17	93.10	31.10
NegLabel	90.22	43.56	99.49	1.91	91.64	35.59	95.49	20.53	94.21	25.40
CSP	93.86	25.52	99.60	1.54	92.90	29.32	96.66	13.66	95.76	17.51
CSP+ΔEnergy (Ours)	94.33	21.44	99.72	0.82	92.66	28.87	96.60	13.75	95.83	16.22

Table 6: **Hard OOD detection Results #1:** OOD detection measured by AUROC and FPR95 over 4 different splits of ImageNet-1k. Details of the 4 splits are in Table 8.

Method	Split-1		Split-2		Split-3		Split-4		Avg	
	AUC \uparrow	FPR95 \downarrow								
MCM	97.93	9.17	88.10	56.40	90.34	33.05	98.72	4.73	93.77	25.83
CLIPN	99.38	2.07	97.77	10.55	90.03	36.85	98.83	4.68	96.50	13.53
MSP	77.85	63.60	68.73	83.63	79.10	70.55	82.40	65.52	77.02	70.83
MaxLogit	99.87	0.49	98.06	8.69	90.96	34.34	99.35	2.66	97.06	11.55
Energy	99.88	0.46	98.18	8.40	90.65	35.02	99.36	2.83	97.02	11.68
ReAct	99.34	0.72	97.91	9.33	90.72	35.65	99.12	2.94	96.77	12.16
ODIN	98.78	1.12	98.23	8.18	89.92	37.20	98.76	13.20	96.42	14.92
ΔEnergy (Ours)	99.93	0.37	99.00	5.16	91.14	30.09	99.40	2.83	97.37	9.61

upper bounded as shown in the following equation:

$$\begin{aligned}
& \max_{\{\theta: |\hat{\mathcal{E}}_{\mathcal{S}}(\theta) - \hat{\mathcal{E}}_{\mathcal{S}}(\theta^*)| \leq \epsilon\}} |\hat{\mathcal{E}}_{\mathcal{T}}(\theta) - \hat{\mathcal{E}}_{\mathcal{S}}(\theta^*)| \\
& \approx \max_{\{\theta: \frac{1}{2}|\theta^\top \hat{\mathbf{H}}_{\mathcal{S}}(\theta^*)\theta| \leq \epsilon\}} \left| \hat{\mathcal{E}}_{\mathcal{T}}(\theta^*) + \frac{1}{2}\theta^\top \hat{\mathbf{H}}_{\mathcal{T}}(\theta^*)\theta - \hat{\mathcal{E}}_{\mathcal{S}}(\theta^*) \right| \\
& \lesssim |\hat{\mathcal{E}}_{\mathcal{T}}(\theta^*) - \hat{\mathcal{E}}_{\mathcal{S}}(\theta^*)| + \max_{\{\theta: \frac{1}{2}|\theta^\top \hat{\mathbf{H}}_{\mathcal{S}}(\theta^*)\theta| \leq \epsilon\}} \frac{1}{2} |\theta^\top \hat{\mathbf{H}}_{\mathcal{T}}(\theta^*)\theta| \quad (34) \\
& \lesssim |\hat{\mathcal{E}}_{\mathcal{T}}(\theta^*) - \hat{\mathcal{E}}_{\mathcal{S}}(\theta^*)| + \max_{\{\theta: \frac{1}{2}|\theta^\top \hat{\mathbf{H}}_{\mathcal{S}}(\theta^*)\theta| \leq \epsilon\}} \frac{1}{2} |\theta^\top [\hat{\mathbf{H}}_{\mathcal{T}}(\theta^*) - \hat{\mathbf{H}}_{\mathcal{S}}(\theta^*) + \hat{\mathbf{H}}_{\mathcal{S}}(\theta^*)]\theta| \\
& \lesssim |\hat{\mathcal{E}}_{\mathcal{T}}(\theta^*) - \hat{\mathcal{E}}_{\mathcal{S}}(\theta^*)| + \max \frac{1}{2} |\theta^\top [\hat{\mathbf{H}}_{\mathcal{T}}(\theta^*) - \hat{\mathbf{H}}_{\mathcal{S}}(\theta^*)]\theta| + \epsilon
\end{aligned}$$

For each image feature \mathbf{z}_I from the source domain, the image features $\tilde{\mathbf{z}}_I$ from the target domain, which share the same label with \mathbf{z}_I , is assumed to satisfy: $\|\mathbf{z}_I - \tilde{\mathbf{z}}_I\|_2 \leq \epsilon_1$. Since we optimize the EBM loss based on the unmasked image features and masked image features, we have the following approximation:

$$|\theta^\top [\hat{\mathbf{H}}_{\mathcal{T}}(\theta^*) - \hat{\mathbf{H}}_{\mathcal{S}}(\theta^*)]\theta| \leq O(\epsilon_1) \quad (35)$$

G More Experiment Results

More experiment details We present experiment details for the baseline models as follows:

Table 7: **Hard OOD detection Results #2.** Comparison with state-of-the-art zero-shot methods on hard OOD detection datasets. In the table, OOD detection is measured by AUROC and FPR95 over 6 hard OOD detection datasets. Details of those datasets can be seen in prior researches (Chen et al., 2024; Ming et al., 2022a).

ID datasets OOD datasets	ImageNet-10		ImageNet-20		ImageNet-10		ImageNet-100		ImageNet-1k		WaterBirds Placesbg	
	ImageNet-20	ImageNet-10	ImageNet-10	ImageNet-100	ImageNet-10	ImageNet-10	ImageNet-100	ImageNet-10	ImageNet-1k	ImageNet-O	WaterBirds	Placesbg
Method	AUROC	FPR95	AUROC	FPR95	AUROC	FPR95	AUROC	FPR95	AUROC	FPR95	AUROC	FPR95
MCM	98.60	6.00	98.09	13.04	99.39	2.50	87.20	60.00	78.59	64.27	87.45	33.62
NegLabel	98.80	5.00	98.04	11.60	99.37	2.50	87.93	49.40	85.78	56.65	87.99	29.16
CSP	99.02	3.30	98.79	3.40	99.33	2.22	89.59	42.40	88.08	51.50	92.88	12.07
Δ Energy (Ours)	99.11	2.80	99.01	3.20	99.40	1.80	91.05	44.80	90.49	41.25	93.45	11.00

Table 8: The 4 ImageNet-1k splits for hard OOD detection following the prior work (Li et al., 2024a). Given are the numbers of classes : training / test samples.

	ID	OOD
Split-1	All dog classes 116: 1856 / 5800	Non-animal classes 166: — / 8300
Split-2	Half of hunting dog classes 30: 480 / 1500	Other 4-legged animal classes 55: — / 2750
Split-3	Mix of common classes 151: 2416 / 7550	Mix of common classes 164: — / 8200
Split-4	First 100 classes 100: 1600 / 5000	Remaining 900 classes 900: — / 45000

Algorithm 1 Algorithm of the proposed EBM method

- 1: **Input:** ID data $\{\mathbf{x}_i, \mathbf{y}_i\}$ ($i \in 1, \dots, N$), ID class names of the K -way classification, masking proportion p , text prompts $\{t_1, t_2, \dots, t_K\}$, hyperparameter λ_0 , and maximum epoch T .
 - 2: **for** $t = 1$ **to** T **do**
 - 3: Calculate the ID image features $\mathbf{z}_I(\mathbf{x}_i)$ and fine-tuned text features $\mathbf{z}_T(t_j; \theta)$ when prompt-tuning the VLM;
 - 4: Compute the cosine similarity between image features $\mathbf{z}_I(\mathbf{x}_i)$ and text features $\mathbf{z}_T(t_j; \theta)$ and denote the text feature with the top-1 similarity as $\mathbf{h}_1(\mathbf{x}_i; \theta)$;
 - 5: Compute the element-wise product $\mathbf{z}_P(\mathbf{x}_i) := \mathbf{z}_I(\mathbf{x}_i) \odot \mathbf{h}_1(\mathbf{x}_i; \theta)$ and generate the mask, denoted as $\mathbf{m}'(\mathbf{x}_i)$, which retains the top p -proportion elements in $\mathbf{z}_P(\mathbf{x}_i)$;
 - 6: Perform masking on the image feature and represent the masked image feature as $\mathbf{z}_I(\mathbf{x}_i) \odot \mathbf{m}'(\mathbf{x}_i)$;
 - 7: Gradient update under the proposed loss as illustrated in Equation 8;
 - 8: **end for**
 - 9: **Output:** Learnable content vectors θ .
-

For zero-shot OOD detection methods such as CSP and NegLabel, all hyperparameters and OOD score calculation procedures are directly adopted from their respective papers (Chen et al., 2024; Jiang et al., 2024) without modification.

For the tuning-based methods, based on the code of CoOp (Zhou et al., 2021), we train models with SGD optimizer with a learning rate of $2e-2$. The batch size is set to 32 for all tuning-based experiments. For the specific hyperparameter for each method, we follow the setting of the original paper.

For the tuning-based methods for improving performances on closed-set data, such as CoOp (Zhou et al., 2021), CoCoOp (Zhou et al., 2022), DPLCLIP (Zhang et al., 2021b), and Bayes-CAL (Zhu et al., 2023b), we use random initialization for context vectors and set the number of context tokens as 16, set the class token position (CTP) as “end”, and set the class-specific context (CSC) as “False”. This configuration has shown the best average performance according to CoOp’s paper. For the DPLCLIP (Zhang et al., 2021b) method, we set the additional hyperparameters of DPLCLIP (Zhang et al., 2021b) as: “mlp_depth=3”, “mlp_width=512”, and “mlp_dropout=0.1”. For the CLIP-Adapter (Gao et al., 2023) method, we adopt image adapter only with the residual ratio of 0.5 for Setup-I and

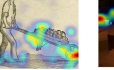
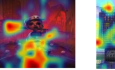
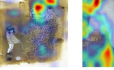
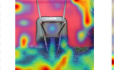
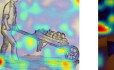
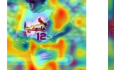
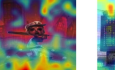
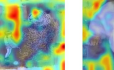
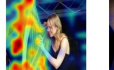
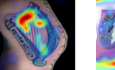
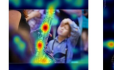
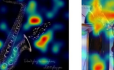
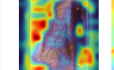
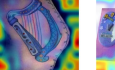
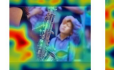
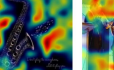
Data	Closed-Set ID	Closed-Set OOD	Open-Set OOD	Closed-Set ID	Closed-Set OOD	Open-Set OOD	Closed-Set ID	Closed-Set OOD	Open-Set OOD
Model	Text Prompt: a photo of a wheelbarrow			Text Prompt: a photo of a baseball player			Text Prompt: a photo of a giant panda		
Original ZS CLIP									
ZS CLIP(+)									
ZS CLIP(-)									
Model	Text Prompt: a photo of a scarf			Text Prompt: a photo of a harp			Text Prompt: a photo of a saxophone		
Original ZS CLIP									
ZS CLIP(+)									
ZS CLIP(-)									

Figure 3: The significant prediction difference between closed-set data and open-set OOD data when vision-language re-alignment is applied to the zero-shot CLIP model (Radford et al., 2021). This difference offers a novel approach to distinguishing between closed-set and open-set classes. Based on the element-wise product between CLIP’s image and text features, the masked ZS CLIP(+) model zeroes out the elements of the image feature where the corresponding values in the product are negative. In contrast, the opposite operation is applied in ZS CLIP(-). It is observed that masking the elements where $P_j < 0$ preserves the model’s original attention, which motivates us to leverage this consistency between the original and masked domains to improve OOD generalization.

0.2 for Setup-II, and we use the bottleneck adapter with a hidden dimension that is 1/4 of the original feature dimension. This hyperparameter configuration has been demonstrated as the most effective for generic image datasets, such as ImageNet, in the original research (Gao et al., 2023).

For tuning-based OOD detection methods, we adopt the recommended hyperparameter settings for LoCoOp, NegPrompt, and GalLoP. For LoCoOp (Miyai et al., 2024b), following the original paper, we set $\lambda = 0.25$. The hyperparameter K is searched over the range [100, 200] for Setup-I, and [2, 3, 4, 5] for Setup-II, based on validation data. For GalLoP, we follow its publicly available source code and adopt the same hyperparameter settings as reported in Table 3 of (Lafon et al., 2024), including configurations for local prompts, global prompts, tokens per prompt, and other relevant settings. In the NegPrompt method (Li et al., 2024a), we follow its source code and train the model using all the classes from the ID dataset and train a shared positive prompt and two shared negative prompts w.r.t. each training ID class. The hyperparameters β and γ are set to 0.1 and 0.05, respectively. In the first stage, CoOp is trained for 100 epochs to obtain the positive prompts. In the second stage, the positive prompts are frozen, and our model is trained for 10 epochs to learn the negative prompts. During the testing phase of LoCoOp, NegPrompt, and GalLoP, we use the GL-MCM score (Miyai et al., 2023) to compute OOD detection results.

For experiments on each method, we repeat 3 times with different random splits to eliminate the effects of randomness. The hyperparameters in each method are selected based on the test accuracy on validation sets.

ΔEnergy based on negative OOD labels The NegLabel (Jiang et al., 2024) and CSP (Chen et al., 2024) methods introduce massive negative labels to boost OOD detection. The extended label space provides a novel perspective to distinguish OOD samples, leveraging extra clues by examining the similarities between images and the extended labels. The CSP method extends the NegLabel by “make up” the OOD label candidates, which are not standard class names but beneficial for the process.

Table 9: Ablations on the hyperparameter c . Δ Energy achieves the overall best performance on both AUROC and FPR95 when $c = 2$.

Data	c=1		c=2		c=3		c=4		c=5		c=6	
	FPR	AUROC										
ID VS Open-Set OOD	49.60	86.46	46.40	87.10	47.23	86.85	47.93	86.44	48.13	86.06	49.97	85.69
Closed-set OOD VS Open-Set OOD	66.54	78.49	67.16	78.68	68.30	78.43	68.40	78.07	69.04	77.79	69.27	77.50

Table 10: Performance of ImageNet-1K-trained model on the test sets with covariate shifts (such as ImageNet_V2, ImageNet_R, ImageNet_A, and ImageNet_S) and concept shifts (such as ImageNet-Superclass).

Dataset	ImageNet (ID)	ImageNet_V2	ImageNet_R	ImageNet_A	ImageNet_S	ImageNet-Superclass	Avg OOD Acc
CLIP	68.80	73.97	46.09	47.77	60.90	33.18	52.38
CoOp	71.86	76.00	48.34	50.13	64.23	36.90	55.12
CoCoOp	71.10	76.18	48.75	50.63	64.07	37.17	55.36
CoOp+EBM (Ours)	71.70	77.10	49.02	51.35	64.78	38.24	56.10

Thus, we also extend our Δ Energy method to CSP, leveraging the informative information from extra OOD labels. Let \mathcal{Y}_{in} denote the ID labels and \mathcal{Y}_{OOD} denote the OOD labels. Thus, Δ Energy is calculated as follows:

$$\Delta\text{Energy}(\mathbf{x}_i) = \Delta\text{Energy}(\mathbf{x}_i; \mathcal{Y}_{\text{in}}) - \Delta\text{Energy}(\mathbf{x}_i; \mathcal{Y}_{\text{OOD}}) \quad (36)$$

Ablations on the hyperparameter c We conduct ablation studies on the hyperparameter c , focusing on its effect on the discrimination between closed-set data and open-set OOD data using ImageNet-1k. The AUROC and FPR95 performances are reported in Table 9. The results demonstrate that: 1) There is a trade-off between the AUROC and FPR95. 2) Δ Energy achieves the overall best performance on both AUROC and FPR95 when $c = 2$. Therefore, unless otherwise specified, we set $c = 2$ in Δ Energy for all experiments.

OOD generalization performance under concept shift We conduct experiments on the concept-shifted ImageNet-Superclass dataset (Xiao et al., 2024; Santurkar et al., 2020), where each image is annotated with its corresponding superclass label. For the superclass labels, we use the open-source annotations provided in https://github.com/s-kumano/imagenet-superclass/blob/main/superclass_names.txt. In Table 10, we report the performance of our ImageNet-1K-trained model on test sets annotated with superclasses. From Table 10, our EBM-based method outperforms baseline models under both covariate and concept shifts. These results demonstrate the effectiveness of our proposed approach in learning domain-invariant features, thereby enhancing the model’s ability to generalize under various distribution shifts.

Fine-tuning accuracy of the proposed EBM on standard datasets used in CLIP We also evaluate the effect of the proposed EBM loss on fine-tuning accuracy across 11 standard datasets used in CLIP. We implement the EBM loss on PromptSRC and train the models using 16-shot settings with a ViT-B/16 backbone. We train 50 epochs for Imagenet and 200 epochs for other datasets with SGD, following the same training setup as in PromptSRC. The EBM hyperparameter was set to $p\% = 0.6$, and we searched over the values of $\{0.1, 0.5, 1.0, 2.0\}$.

The performance results are reported in Table 11, demonstrating that the proposed EBM method further improves test accuracy on PromptSRC. Since the objective of EBM is to minimize $\mathcal{L}_{\Delta E}$, it encourages the model to make equally high-confidence predictions for both the original and partially masked features, thus facilitating the learning of domain-invariant features between the original domain and the masked domain. The improvements observed in Table 11 empirically suggest that regularization on masked features effectively enhances the model’s generalization performance.

H Limitations and Future Work

As demonstrated in Theorems 3.2-3.3 and B.1, our method outperforms the MCM approach by enlarging the difference between the ID and open-set OOD samples. The empirical results in Tables 1–2 and Tables 6–7 further support our theoretical findings. While our method also improves performance on conventional OOD detection benchmarks, the gains are less pronounced compared to the hard OOD scenarios. This may be due to the reduced impact of amplifying the distinction between

Table 11: Performances of fine-tuning accuracy on 11 standard datasets used in CLIP.

Data	ImageNet	Caltech101	OxfordPets	Cars	Flowers102	Food101	Aircraft	SUN397	DTD	EuroSAT	UCF101	Avg
CLIP	66.7	92.2	88.4	65.5	70.7	84.8	24.8	62.3	44.1	48.3	64.7	64.8
CoOp	71.7	95.6	91.9	83.1	97.1	84.2	43.4	74.7	69.9	84.9	82.2	79.9
CoCoOp	71.0	95.2	93.3	71.6	87.8	87.2	31.2	72.2	63.0	73.3	78.1	74.9
MaPLe	72.3	96.0	92.8	83.6	97.0	85.3	48.4	75.5	71.3	92.3	85.0	81.8
PLOT	72.6	96.0	93.6	84.6	97.6	87.1	46.7	76.0	71.4	92.0	85.3	82.1
PromptSRC	73.2	96.1	93.7	83.8	97.6	86.5	50.8	77.2	72.7	92.4	86.5	82.8
Ours	73.6	96.5	94.4	85.3	98.2	87.6	51.3	77.3	73.3	93.5	86.7	83.4

Table 12: Comparison of computational efficiency between our method and prior approaches.

Category	Method	Time	GPU (MB)	Batch Size
Zero-shot	MCM	17s	1706	100
	ΔEnergy (Ours)	18s	1706	100
Fine-tuning	CoOp	18min	7658	32
	LoCoOp	25min	8320	32
	GalLoP	140min	47492	32
	EBM (Ours)	18min	7756	32

ID and OOD samples when the inherent difference between ID and open-set OOD samples is already substantial. Future work may explore strategies to further enhance ΔEnergy by incorporating CSP’s informative negative labels.

I Computation Efficiency

The proposed zero-shot OOD detection method does not require fine-tuning of VLM parameters. Instead, it introduces a novel post-hoc scoring function to identify open-set OOD samples. All computations are performed in the latent space during the alignment between vision and language representations, enabling improved OOD detection performances with comparable inference time and computational cost to existing methods such as MCM and raw energy scores. Compared to methods like NegLabel and CSP, ΔEnergy does not rely on additional negative labels, making it more computationally efficient. For tuning-based approaches, our proposed EBM method enables joint optimization for both OOD generalization and OOD detection by the novel optimization objective as defined in Equation 8. It re-aligns vision-language representations in the latent space without introducing extra prompts, as required by vanilla CoOp (Zhou et al., 2021), thereby it is more efficient over methods such as LoCoOp (Miyai et al., 2024b) and GalLoP (Lafon et al., 2024). A detailed comparison of computation cost is provided in Table 12. Here, GalLoP is trained using four NVIDIA RTX 4090 GPUs, while all other experiments are conducted on a single NVIDIA RTX 4090 GPU.